
Mechanisms of Signal Transduction:

# The Gα12/13 Family of Heterotrimeric G Proteins and the Small GTPase RhoA Link the Kaposi Sarcoma-associated Herpes Virus G Protein-coupled Receptor to Heme Oxygenase-1 Expression and Tumorigenesis

María José Martín, Tamara Tanos, Ana Belén García, Daniel Martin, J. Silvio Gutkind, Omar A. Coso and Maria Julia Marinissen

*J. Biol. Chem. 2007, 282:34510-34524.*
*doi: 10.1074/jbc.M703043200 originally published online September 19, 2007*

THE JOURNAL OF BIOLOGICAL CHEMISTRY VOL. 282, NO. 47, pp. 34510–34524, November 23, 2007
Printed in the U.S.A.

# The $G\alpha_{12/13}$ Family of Heterotrimeric G Proteins and the Small GTPase RhoA Link the Kaposi Sarcoma-associated Herpes Virus G Protein-coupled Receptor to Heme Oxygenase-1 Expression and Tumorigenesis*

Received for publication, April 11, 2007, and in revised form, September 14, 2007 Published, JBC Papers in Press, September 19, 2007, DOI 10.1074/jbc.M703043200

**María José Martín[‡1], Tamara Tanos[§2], Ana Belén García[‡3], Daniel Martin[¶], J. Silvio Gutkind[¶], Omar A. Coso[§], and Maria Julia Marinissen[‡4]**

*From the [‡]Instituto de Investigaciones Biomédicas A. Sols, Departamento de Bioquímica, Facultad de Medicina, Universidad Autónoma de Madrid, Madrid 28029, Spain, the [§]Departamento de Fisiología y Biología Molecular, Facultad de Ciencias Exactas y Naturales, Universidad de Buenos Aires, IFYBYNE-CONICET, 1428 Buenos Aires, Argentina, and [¶]Oral and Pharyngeal Cancer Branch, NIDCR, National Institutes of Health, Bethesda, Maryland 20892*

**Heme oxygenase-1 (HO-1), an inducible enzyme that metabolizes the heme group, is highly expressed in human Kaposi sarcoma lesions. Its expression is up-regulated by the G protein-coupled receptor from the Kaposi sarcoma-associated herpes virus (vGPCR). Although recent evidence shows that HO-1 contributes to vGPCR-induced tumorigenesis and vascular endothelial growth factor (VEGF) expression, the molecular steps that link vGPCR to HO-1 remain unknown. Here we show that vGPCR induces HO-1 expression and transformation through the $G\alpha_{12/13}$ family of heterotrimeric G proteins and the small GTPase RhoA. Targeted small hairpin RNA knockdown expression of $G\alpha_{12}$, $G\alpha_{13}$, or RhoA and inhibition of RhoA activity impair vGPCR-induced transformation and *ho-1* promoter activity. Knockdown expression of RhoA also reduces vGPCR-induced VEFG-A secretion and blocks tumor growth in a murine allograft tumor model. NIH-3T3 cells expressing constitutively activated $G\alpha_{13}$ or RhoA implanted in nude mice develop tumors displaying spindle-shaped cells that express HO-1 and VEGF-A, similarly to vGPCR-derived tumors. RhoAQL-induced tumor growth is reduced 80% by small hairpin RNA-mediated knockdown expression of HO-1 in the implanted cells. Likewise, inhibition of HO-1 activity by chronic administration of the HO-1 inhibitor tin protoporphyrin IX to mice reduces RhoAQL-induced tumor growth by 70%. Our study shows that vGPCR induces HO-1 expression through the $G\alpha_{12/13}$/RhoA axes and shows for the first time a potential role for HO-1 as a therapeutic target in tumors where RhoA has oncogenic activity.**

Heme oxygenase-1 is an inducible and ubiquitous 32-kDa enzyme that controls heme metabolism and iron levels by catalyzing the degradation of the heme group (iron protoporphyrin IX). The products of this enzymatic reaction are the physiological messenger molecule carbon monoxide, free iron, and biliverdin, the last being subsequently reduced to the antioxidant bilirubin (1). The regulation of HO-1 activity depends primarily on the control of HO-1 expression at the transcriptional level (1–3), and it is triggered by a variety of stress-inducing stimuli, antioxidants, growth factors, and hormones (4–7). Because of the antioxidant properties of the heme metabolism products, HO-1 has been considered a cytoprotector molecule involved in several physiological responses against inflammation and oxidative and cellular stress (2). However, an increasing number of studies have now expanded this notion defining HO-1 as an important regulator of the physiology of the vasculature, endothelial cell cycle control, proliferation, vascular endothelial growth factor (VEGF)[5] secretion, angiogenesis, and tumorigenesis (3, 8–14). A recent study shows that HO-1 expression is induced in endothelial cells infected by the angiogenic and oncogenic Kaposi sarcoma-associated herpesvirus (KSHV) and that the enzyme is highly expressed in biopsy tissues from oral AIDS-Kaposi sarcoma lesions (15).

Kaposi sarcoma (KS) is the most frequent type of tumor in AIDS patients. The multifocal angioproliferative lesions are formed by spindle cells derived from endothelial cells transformed by the KSHV (16). Several experimental strategies using animal models revealed that the product of the *orf* 74 from the KSHV genome, a G protein-coupled receptor (vGPCR), plays a key role in the development of KSHV-induced oncogenesis (16–19). Indeed, although only few cells in KS-like lesions express the vGPCR (17), down-regulation of the receptor in

* This work was supported by a grant from "Fundación Médica Mutua Madrileña" and by "Ministerio de Educación y Ciencia," Spain, Grant SAF2005-03020. The costs of publication of this article were defrayed in part by the payment of page charges. This article must therefore be hereby marked "*advertisement*" in accordance with 18 U.S.C. Section 1734 solely to indicate this fact.

[1] Recipient of a collaboration fellowship from the Ministerio de Educación y Ciencia, Spain. The visit to Dr. Gutkind's laboratory (NIDCR, National Institutes of Health) was supported by Fundación Mutua Madrileña, Spain.

[2] This author's visit to our laboratory in Spain was supported by a grant from the Fundacion Mutua Madrileña, Spain.

[3] A fellow from FINNOVA, Comunidad de Madrid.

[4] To whom correspondence should be addressed: Instituto de Investigaciones Biomédicas A. Sols, Dept. de Bioquimica, Facultad de Medicina, Universidad Autonoma de Madrid, Arzobispo Morcillo 4, Madrid 28029, Spain. Tel.: 34-91-497-5464; E-mail: mjmarinissen@iib.uam.es.

[5] The abbreviations used are: VEGF, vascular endothelial growth factor; KSHV, Kaposi sarcoma-associated herpesvirus; GPCR, G protein-coupled receptor; vGPCR, G protein-coupled receptor from the Kaposi sarcoma-associated herpes virus; HA, hemagglutinin; shRNA, small hairpin RNA; DMEM, Dulbecco's modified Eagle's medium; SnPP, tin protoporphyrin IX; PBS, phosphate-buffered saline; GAPDH, glyceraldehyde-3-phosphate dehydrogenase; DAPI, 4′,6-diamidino-2-phenylindole; RT, reverse transcription; GFP, green fluorescent protein; KS, Kaposi sarcoma; SRE, serum response element.

these cells results in diminished expression of angiogenic factors and ultimately tumor regression (20, 21). vGPCR is homologous to the mammalian interleukin-8 receptor CXCR2 (22) but contains a D142V mutation in the highly conserved Asp-Arg-Tyr (DRY) motif in homologue mammalian GPCRs, which enables its constitutive, ligand-independent activity. Expression of vGPCR induces transformation in fibroblasts, angiogenesis in endothelial cells (23), and KS-like angioproliferative lesions in mice (17, 23, 24).

We have recently shown that vGPCR induces HO-1 mRNA and protein levels in fibroblasts and endothelial cells and that these increased levels correlate with increased cell proliferation and survival, as well as increased VEGF-A expression, one of the determinant events in KS development. Additionally, inhibition of HO-1 expression or activity critically impairs vGPCR-induced tumorigenesis in allograft tumor animal models (25). Despite the implication of HO-1 as a vGPCR downstream target, the nature of the molecular pathways connecting the receptor to HO-1 expression remains unknown. New studies show that vGPCR contributes to KS development by switching on a complex network of signaling pathways, including the direct or autocrine/paracrine activation and expression of receptors, cytokines, signaling molecules, and transcription factors (18, 26). As other GPCRs, vGPCR activates downstream effectors by coupling to distinct $\alpha$ subunits of heterotrimeric G proteins (27–29). Among these effectors are the monomeric or small G proteins of the Rho family represented by RhoA, Rac1, and Cdc42 (30). Indeed, Rac1 is activated by the receptor and mediates vGPCR-induced transformation in cells and tumorigenesis in animal models (28, 31), whereas RhoA is required for vGPCR-induced NF$\kappa$B activation and interleukin-8 secretion (29). Although it is known that some GPCRs induce HO-1 expression (5, 32–34), the nature of the molecules connecting these receptors to HO-1 expression has not been established.

In this study, we show that expression of constitutively activated $G\alpha_{12}$ and $G\alpha_{13}$ subunits mimicked vGPCR-induced HO-1 expression and transformation and that vGPCR activates HO-1 and transformation through both G $\alpha$ subunits. Our data indicate that vGPCR activates the small GTPase RhoA, a known downstream effector of $G\alpha_{112/13}$, and that reduced expression or inhibition of RhoA impairs vGPCR-induced VEGF expression and secretion, cell survival and proliferation, and transformation both in cell culture and in a murine allograft tumor model. Moreover, $G\alpha_{13}$- and RhoA-induced tumorigenesis are dramatically impaired when HO-1 expression or activity is inhibited. These data show that the $G\alpha_{12/13}$/RhoA signal transduction pathway is an important mediator of vGPCR-induced tumor growth and demonstrate the participation of HO-1 in this process. These findings uncover a more extensive role of HO-1 in tumorigenesis and suggest that the enzyme can be a potential therapeutic target in the treatment not only of KS but also of tumors where RhoA is oncogenic.

## EXPERIMENTAL PROCEDURES

*DNA Constructs*—The plasmids pHO1-Luc containing a 5-kb human HO-1 promoter upstream of a luciferase gene and pVEGF-Luc have been previously described (35, 36). pCEFL-AU5-vGPCR, pCDNAIII-$\beta$-galactosidase, pCEFL-green fluorescent protein (GFP), pCDNAIII-$G\alpha_{12}$QL, pCEFL-HA-$G\alpha_{13}$QL, pCDNAIII-$G\alpha_{q}$QL, pCDNAIII-$G\alpha_{i}$QL, pCDNAIII-$G\alpha_{s}$QL, pCEFL-HA-m2, pCEFL-HA-$G_{13i5}$, pCEFL-HA-$G_{qi5}$, pCEFL-p115RGS-D, pCEFL-AU5-RhoAQL, pCEFL-HA-HO-1, pCEFL-AU1-PDZRhoGEF, pCEFL-RhoN19, pEF-C3, pCEFL-AU5-Rac1QL, pNF$\kappa$B-Luc, and pSshRNAHO-1 have been already described (25, 37–40). pCEP4, a plasmid carrying a hygromycin resistance gene, was commercially purchased (Invitrogen). Plasmids carrying shRNAs sequences were constructed by inserting double-stranded shRNA oligonucleotides in the pSilencer 1.0-U6 plasmid following the manufacturer's instructions (Ambion). The plasmids pSshRNARho1 and pSshRNARho2 carrying shRNA sequences for RhoA were engineered by annealing the following single strand oligonucleotides: 5′-GACATGCTTGCTCATAGTCTTCAAGAGAGACTATGAGCAAGCATGTCTTTTTT and 3′-AATTAAAAAAGACATGCTTGCTCATAGTCTCTCTTGAAGACTATGAGCAAGCATGTCGGCC for pSshRNARho1 (41) and 5′- GAAACTGGTGATTGTTGGTTTCAAGAGAACCAACAATCACCAGTTTCTTTTTT and 3′-AATTAAAAAAGAAACTGGTGATTGTTGGTTCTCTTGAAACCAACAATCACCAGTTTCGGCC for pSshRNARho2. pSshRNA$G\alpha_{13.1}$ and pSshRNA$G\alpha_{13.2}$ were constructed using the following sequences: shRNA$G\alpha_{13.1}$, 5′- GTCCAAGGAGATCGACAAATTCAAGAGATTTGTCGATCTCCTTGGACTTTTTT and 3′-AATTAAAAAAGTCCAAGGAGATCGACAAATCTCTTGAATTTGTCGATCTCCTTGGACGGCC; shRNA$G\alpha_{13.2}$, 5′-GCAACGTGATCAAAGGTATTTCAAGAGAATACCTTTGATCACGTTGCTTTTTT and 3′-AATTAAAAAAGCAACGTGATCAAAGGTATTCTCTTGAAATACCTTTGATCACGTTGCGGCC. $G\alpha_{12}$ shRNA oligonucleotides (shRNA$G\alpha_{12}$) have been previously described (42). A control construct carrying a "scramble" sequence, pSshRNAscramble, was made, annealing the oligonucleotides 5′-GCTAATTCCGAATCGGTCTTTCAAGAGAAGACCGATTCGGAATTAGCTTTTTT and 3′-AATTAAAAAAGCTAATTCCGAATCGGTCTTCTCTTGAAAGACCGATTCGGAATTAGCGGCC.

*Cell Lines and Transfections*—Transient transfections of NIH-3T3 and HEK (human embryonic kidney) 293T were performed using the Lipofectamine Plus reagent (Invitrogen). HEK 293T cells were cultured in Dulbecco's modified Eagle's medium (DMEM) supplemented with 10% fetal bovine serum. NIH-3T3 fibroblasts were maintained in DMEM (Invitrogen) supplemented with 10% calf serum. NIH-vGPCR cells were prepared as described (25). Stable transfection of NIH-3T3 cells was performed using the calcium phosphate technique (40). Cells were plated at 20% confluence in 10-cm plates and transfected with 10 $\mu$g of pCEFL (NIH-3T3c), pCEFL-HA-m2 (NIH-m2), pCEFL-HA-$G\alpha_{13}$QL (NIH-$G\alpha_{13}$QL), or pCEFL-AU5-RhoAQL (NIH-RhoAQL). Stably transfected cells were selected with 750 $\mu$g/ml G418 (Promega). NIH-m2 cells were further transfected with 5 $\mu$g of pCEFL-$G_{13i5}$ (NIH-m2-$G_{13i5}$) or pCEFL-$G_{qi5}$ (NIH-m2-$G_{qi5}$) along with 100 ng of pCEP4 to allow selection by hygromycin. NIH-RhoAQL cells were transfected with 5 $\mu$g of pSshRNAHO-1 (NIH-RhoAQL$_{shHO-1}$) and 100 ng of pCEP4. NIH-vGPCR cells were transfected with 100 ng of pCEP4 and 5 $\mu$g of pSshRNARho1 or pSshRNARho2 (NIH-vGPCR$_{shRho1}$, NIH-vGPCR$_{shRho2}$). NIH-vGPCR cells were also stably transfected with 5 $\mu$g of pSshRNA$G\alpha_{13.1}$,

pSshRNAG$\alpha_{13.2}$, pSshRNAG$\alpha_{12}$, or pSshRNAscramble (NIH-vGPCR$_{shG13.1}$, NIH-vGPCR$_{shG13.2}$, NIH-vGPCR$_{shG12}$, or NIH-vGPCR$_{shScram}$, respectively). Transfected cells were selected with 200 μg/ml hygromycin B from *Streptomyces* (Sigma).

*Gene-specific Real Time PCR*—Total RNA from cells was extracted by homogenization in TRIzol (Invitrogen). Briefly, cells were grown to 80% confluence, serum-starved for 24 h, washed with cold PBS, and lysed in TRIzol according to the manufacturer's indications. Equal amounts of RNA (1 μg) were reverse-transcribed to obtain cDNA with the Enhanced Avian First Strand Synthesis kit (Sigma). Real time PCR was performed using the ABI prism 7700 sequencer detector system and Qiagen's Quantitect SYBR Green PCR kit (Qiagen, Chatsworth, CA), following the manufacturer's protocol. In brief, the reaction mixture (50-μl total volume) contained 500 ng of cDNA, gene-specific forward and reverse primers for each gene at 1 mM final concentration, and 25 μl of Quantitect SYBR Green PCR Master Mix. The real time cycler conditions were as follows: PCR initial activation step at 95 °C for 10 min, 40 cycles each of melting at 95 °C for 15 s, and annealing/extension at 60 °C for 1 min. A negative control without template was included in parallel to assess the overall specificity of the reaction. The PCR products were analyzed on a 1.2% agarose gel to confirm the size of the amplified product. After PCR, a comparative delta cycle threshold method was used to determine the relative amounts of specific gene and actin mRNA. The sequences of the primers used were as follows: HO-1, 5′-CAACAGTGGCAGTGGGAATTT and 3′-CCAGGCAAGATTCTCCCTTAC; GAPDH, 5′-TCCATCACAACTTTGGCATTG and 3′-TCACGCACAAGCTTTCCA; β-actin 5′-AGTACTCCGTGTGGATCGGC and 3-AGGTCGTCTACACCTAGTCG.

*Analysis of mRNA Levels by Semiquantitative Reverse Transcription-PCR*—Total RNA from cells was obtained by extraction in TRIzol (Invitrogen). Total RNA from tumors was obtained by homogenizing the tissue in TRIzol with a Teflon homogenizer followed by sonication. Equal amounts of RNA (1 μg) were reverse-transcribed to obtain cDNA with the Enhanced Avian First Strand Synthesis kit (Sigma). PCRs were performed using the Ready Mix RedTaq PCR reactive mix (Sigma). HO-1 oligonucleotides described above were used to amplify a 106-bp HO-1 fragment. A vGPCR fragment was amplified using the oligonucleotides 5′-GCGAATTCACCATGGCGGCCGAGGATTTCCTAAC and 3′-GCGCGGCCGCCTACGTGGTGGCGCCGGACATGA. The three splice variants of VEGF-A were amplified using 5′-CTGCTCTCTTGGGTGCACTGG and 3′-ACCGCCTTGGCTTGTCACAT primers (40). Expected product sizes were 431, 563, and 635 bp, corresponding to the VEGF120, VEGF164, and VEGF188 splice variant isoforms (35). A 982-bp DNA fragment from the coding sequence for AU5-RhoAQL was amplified by the oligonucleotides AU5 (5′-ATGGGATCCACCGACTTCTACC) and RhoA (3′-CTTCCCACGTCTAGCTTGCAGA). HA-G$\alpha_{13}$QL was amplified using HA (5′-TACCCATATGACGTACCGGATTACGCA) and G$\alpha_{13}$ (3′-GAGATTCTGTAAGGCGATTG). A fragment of 102 bp from the GAPDH housekeeping gene was amplified in parallel to all reactions to ensure that equal amounts of starting cDNA were used in each reaction. After an initial denaturalization step of 2 min at 94 °C, amplification of each cDNA was performed in 22–34 cycles (in increments of 2), to detect the linear amplification phase. Reactions were set at 28 cycles, which also allowed detection of basal HO-1 mRNA levels in control cells. The same amount of cycles was used for VEGF-A, AU5-RhoA, HA-G$\alpha_{13}$, and GAPDH, using a thermal profile of 30 s at 94 °C, 30 s at 58 °C, and 30 s at 72 °C. The PCR products were detected by electrophoresis in agarose gels and fluorescence under UV light upon ethidium bromide staining.

*Luciferase Reporter Assays*—NIH-3T3 cells were transfected with different expression plasmids together with 0.1 μg of the indicated reporter plasmid and 100 ng of p*Renilla*-null (Promega Corp.) per well in 6-well plates. In all cases, the total amount of plasmid DNA was adjusted with pcDNAIII-β-galactosidase or pCEFL-GFP. When indicated, cells were starved and treated for 24 h with 100 μM tin protoporphyrin IX (SnPP) (Frontier Scientific Europe Ltd.) dissolved in 0.1 N NaOH in PBS, pH 7.5. Firefly and *Renilla* luciferase activities present in cellular lysates were assayed using the Dual Luciferase reporter system (Promega), and light emission was quantified using a BG1 Optocomp I, GEM Biomedical luminometer (Sparks, NV).

*Western Blot*—Cells were lysed, and extracted proteins were resolved in 12% SDS-polyacrylamide gels and transferred to polyvinylidene difluoride membranes. Endogenous HO-1 and transfected HA-HO-1 were detected by specific rabbit polyclonal anti-HO-1 (Stressgen Bioreagents) and mouse monoclonal anti-HA antibodies (Covance). RhoA and AU5-RhoA were detected by anti-RhoA (Santa Cruz Biotechnology, Inc., Santa Cruz, CA) and anti-AU5 (Covance) antibodies, respectively. G$\alpha_{12}$ and G$\alpha_{13}$ were detected using G$\alpha_{12}$ SC-20 and G$\alpha_{13}$ A-13 antibodies from Santa Cruz Biotechnology. As a loading control, α-actin was detected using a rabbit polyclonal antibody (Sigma). Membranes were stripped with Restore Western blot stripping buffer (Pierce), following the manufacturer's indications. Proteins were visualized by enhanced chemiluminescence detection (Amersham Biosciences) using goat anti-mouse and anti-rabbit IgGs coupled to horseradish peroxidase as the secondary antibody (Amersham Biosciences).

*Focus-forming Assays*—NIH-3T3 cells were transfected by the calcium phosphate precipitation technique with 1 μg of each indicated expression plasmid as previously described (40). The day after transfection, cells were washed three times with DMEM and kept in DMEM supplemented with 5% calf serum alone or with 100 μM SnPP for 2–3 weeks until foci were scored. Alternatively, $5 \times 10^4$ NIH-3T3c, NIH-vGPCR, NIH-RhoAQL, NIH-vGPCR$_{shRho2}$, or NIH-RhoAQL$_{shHO-1}$ cells were seeded on a 70% confluent monolayer of NIH-3T3 cells and cultured as above until foci were detected. Cells were fixed with methanol for 30 min, washed with water, dried, and stained with Giemsa (Sigma).

*Rho Activation Assay*—Rho activity in cultured cells was assessed by a modified Rho binding domain assay as already described (43). Briefly, NIH-3T3 cells were transfected with the indicated plasmids, and after serum starvation for 24 h, cells were lysed at 4 °C in a buffer containing 20 mM HEPES, pH 7.4, 0.1 M NaCl, 1% Triton X-100, 10 mM EGTA, 40 mM glycerophosphate, 20 mM $MgCl_2$, 1 mM $Na_3VO_4$, 1 mM dithiothreitol, 10 μg/ml aprotinin, 10 μg/ml leupeptin, and 1 mM phenylmeth-

ylsulfonyl fluoride. Lysates were incubated with glutathione *S*-transferase-rhotekin-Rho binding domain previously bound to glutathione-Sepharose beads and washed four times with lysis buffer. Associated GTP-bound forms of Rho were released with protein loading buffer and revealed by Western blot analysis using a monoclonal antibody against RhoA (Santa Cruz Biotechnology).

*Indirect Immunofluorescence*—NIH-3T3 cells were seeded on glass coverslips and transfected with Lipofectamine Plus reagents (Invitrogen). Cells were serum-starved for 24 h, washed twice with 1× PBS, and then fixed and permeabilized with 4% formaldehyde and 0.05% Triton X-100 in 1× PBS for 10 min. After washing with PBS, cells were blocked with 1% bovine serum albumin and incubated with anti HO-1 (Stressgen Bioreagents) or anti-AU5 antibodies (Covance) as primary antibodies for 1 h. Following incubation, cells were washed three times with 1× PBS and then incubated for an additional 1 h with the corresponding secondary antibodies (1:200) conjugated with tetramethylrhodamine B isothiocyanate and fluorescein isothiocyanate (Molecular Probes). When indicated, cells were incubated with AlexaFluor 594 phalloidin (1:40) for 30 s (Invitrogen) to stain actin filaments. Cells were washed three times with 1× PBS and stained with DAPI (1 $\mu$g/ml) (Molecular Probes) in the last wash. Coverslips were mounted in Fluorosafe mounting medium (Calbiochem) and viewed using a Nikon Eclipse TE2000-S photomicroscope equipped with epifluorescence.

*Immunohistochemistry*—Tumor tissues were removed and fixed in 4% paraformaldehyde in 1× PBS, transferred to 70% ethanol, and embedded in paraffin. Sections were deparaffinized in SafeClear and hydrated through graded alcohols and distilled water. Antigens were retrieved by heat in 10 mM citrate buffer, and sections were incubated with the anti-HO-1 (Stressgen Bioreagents) and the anti-VEGF (Santa Cruz Biotechnology) antibodies (1:500). Slides were incubated with biotinylated anti-mouse antibody for 1 h and then with ABC (avidin and biotinylated peroxidase complex) solution for 30 min (Vectastain ABC kit; Vector Laboratories). Peroxidase reaction was developed using a 3,3′-diaminobenzidine and hydrogen peroxide solution (Sigma) under microscope control. Parallel slides were stained with hematoxylin-eosin. Slides were dehydrated and mounted in Permount mounting medium (Fisher).

*In Vitro Apoptosis Assay*—Apoptosis was determined by staining cells with propidium iodide. Briefly, cells were plated in 6-well plates (250,000 cells/well), serum-starved for 48 h, and simultaneously treated with vehicle or 100 $\mu$M SnPP in 0.1 N NaOH in PBS, pH 7.5. Attached cells were harvested by centrifugation, washed with PBS, and resuspended in 50 g/ml propidium iodide in 0.1% sodium citrate with 0.1% Triton X-100 for 20 min at 4 °C. Cells were then analyzed by flow cytometry, and the sub-$G_0/G_1$ fraction was used as a measure of the apoptotic percentage. DNA content of cells was quantified on a BD Biosciences FACScan and analyzed using Cell Quest software (Immunocytometry system; BD Biosciences).

*[$^3$H]Thymidine Incorporation*—Cells were seeded in 24-well plates, and after overnight growth, they were serum-starved for 48 h, followed by a 2-h pulse incubation with 0.5 $\mu$Ci/ml [$^3$H]thymidine. Monolayers were washed three times with PBS, twice with 10% trichloroacetic acid, and lysed in 1 N NaOH. Aliquots were counted by liquid scintillation, and parallel protein samples were quantified (Bio-Rad) for normalization.

*VEGF-A Secretion*—NIH-3T3c, NIH-vGPCR, NIH-$G\alpha_{13}$QL, NIH-RhoAQL, NIH-$vGPCR_{shRho2}$, and NIH-$RhoAQL_{shHO-1}$ cells were plated at similar densities in 6-well plates. After overnight growth, cells were serum-starved and left untreated (control) or treated with 100 $\mu$M SnPP for 24 h. An enzyme-linked immunosorbent assay kit was used for specific VEGF-A detection in 100 $\mu$l of cell culture supernatant, according to the manufacturer's protocol (RayBiotech, Inc.). Data were normalized by protein concentration in each well. Proteins were quantified with the DC protein assay (Bio-Rad).

*Tumor Allografts in Athymic Nude Mice*—NIH-RhoAQL, NIH-$RhoAQL_{shHO-1}$, NIH-vGPCR, and NIH-$vGPCR_{shRho2}$ cell lines were harvested, washed, counted, and resuspended in PBS. $1 \times 10^6$ viable cells were transplanted subcutaneously into the right flank of 7-week athymic (nu/nu) nude female mice. When tumors were noticeable and reached a diameter of ~3 mm, mice were randomly separated in two groups and treated with vehicle ($n = 5$) or SnPP (10 $\mu$mol/kg of body weight dissolved in 0.1 N NaOH in PBS, pH 7.5, $n = 5$) administered subcutaneously in the right flank, every other day, for the indicated times. Tumor volume and body weight were measured every other day during the period of investigation. Tumor volumes ($V$) were determined by the formula $V = L \times W^2 \times 0.5$, $L$ being the longest cross-section and $W$ the shortest.

*Image Analysis and Quantification*—Different band intensities corresponding to ethidium bromide detection of DNA samples or Western blot detection of protein samples were quantified using the Scion Image program (available on the World Wide Web).

*Statistical Analysis*—Means from test samples were compared against means from controls in all experiments, and statistical differences were calculated by the two-tailed impaired $t$ test. All differences shown had a $p$ value of $\leq 0.05$ (*), which was considered statistically significant.

## RESULTS

*The $G\alpha_{12/13}$ Family of Heterotrimeric G Proteins Induces Transformation and HO-1 Expression*—It has been shown that the $\alpha$ subunits of the $G\alpha_{12/13}$, $G\alpha_{q/11}$, and $G\alpha_{i/0}$ families of heterotrimeric G proteins can transduce signals initiated by vGPCR (27, 29, 44). Thus, we investigated if any of these subunits *per se* were capable of inducing transformation when compared with vGPCR in a focus formation assay. NIH-3T3 cells were transfected with a negative control plasmid expressing $\beta$-galactosidase, vGPCR, or expression vectors carrying cDNAs encoding for representative members of each G-protein $\alpha$ subunit family in their constitutively active form (QL mutants) (45). As shown in Fig. 1*A*, only cells transfected with $G\alpha_{13}$QL developed foci similarly to cells transfected with vGPCR, whereas a very limited number of foci where observed in $G\alpha_q$-transfected cells, and no foci appeared in $G\alpha_i$-transfected cells. Since previous observations indicate that $G\alpha_q$ is transforming only under special conditions and cell types (46) and high concentrations can induce cell toxicity (47), we transfected cells with different amounts of the $G\alpha_q$QL (0.1–2.0 $\mu$g).

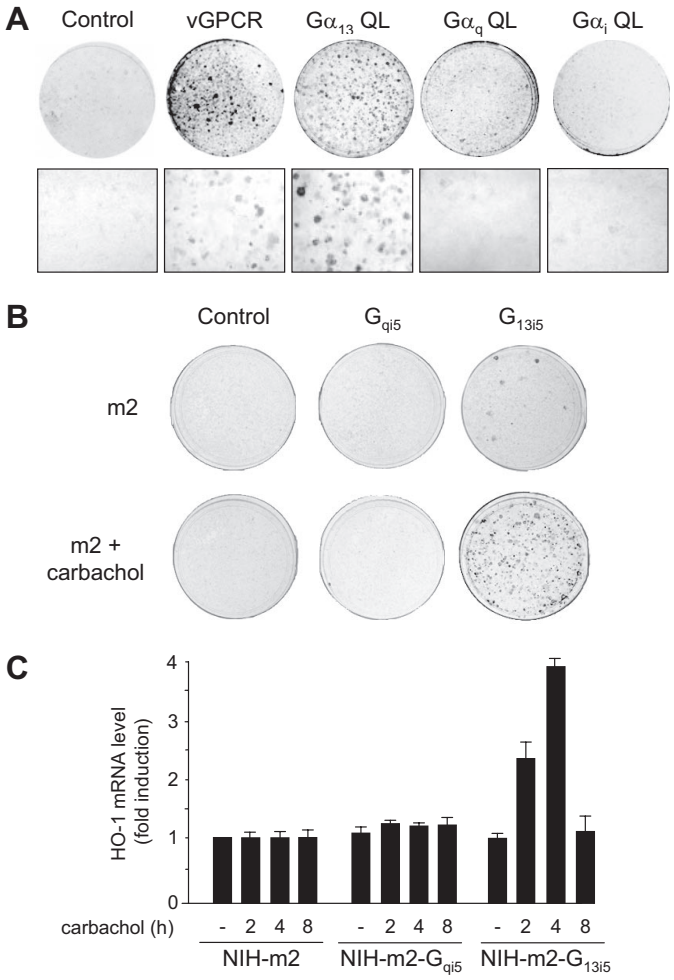


FIGURE 1. **The $G\alpha_{12/13}$ family of heterotrimeric G proteins induce transformation and HO-1 expression.** *A*, NIH-3T3 cells were transfected with 1 $\mu$g of pCEFL-HA-$G\alpha_{13}$QL, pCDNAIII-$G\alpha_q$QL, pCDNAIII-$G\alpha_i$QL, or pCEFL-AU5-vGPCR by the calcium phosphate technique. After 3 weeks, plates were fixed and stained to score formation of foci. Plates shown are representative of three different experiments. *B*, NIH-3T3 cells were transfected by the calcium phosphate technique with 1 $\mu$g of pcDNAIII-$\beta$-galactosidase, pCEFL-HA-m2, and pCEFL-HA-$G\alpha_{13i5}$ or pCEFL-HA-$G\alpha_{qi5}$ as indicated. Cells were treated with 100 $\mu$M carbachol twice a week as indicated. After 3 weeks, plates were fixed and stained to score formation of foci. Plates shown are representative of three different experiments. *C*, NIH-m2, NIH-m2-$G_{13i5}$, and NIH-m2-$G_{qi5}$ cells were serum-starved overnight and treated with 100 $\mu$M carbachol for 2, 4, and 8 h. Total RNA was extracted, and HO-1 mRNA levels were detected by quantitative PCR. Data were analyzed by a comparative delta cycle threshold method. Results indicate mean ± S.E. from triplicates and are representative of three independent experiments.

No foci were detected under any of these conditions (data not shown). To confirm these results, and dissect the isolated effect of receptor-activated $G\alpha_q$ or $G\alpha_{13}$ on transformation and HO-1 expression, we took advantage of previously described $G\alpha_{qi5}$ and $G\alpha_{13i5}$ chimeras, in which the C-terminal region of the $\alpha$ subunits was replaced with the corresponding region of $G\alpha_i$. Co-expression of these chimeras along with the $G\alpha_i$-coupled m2 muscarinic receptor generates a system that can specifically signal downstream from $G\alpha_q$ and $G\alpha_{13}$ and that can be turned on by adding carbachol, a muscarinic receptor synthetic agonist (40, 48). Because m2 receptors and $G\alpha_i$ subunits did not induce transformation or HO-1 expression (40) (data not shown), we transfected NIH-3T3 cells with the m2 receptor alone or in combination with the $G\alpha_{qi5}$ or $G\alpha_{13i5}$ chimeras. Cells were incubated with media containing 1 mM carbachol or vehicle (control), and after 3 weeks, only cells treated with carbachol and transfected with m2 and $G_{13i5}$ generated a significant amount of foci. No transformation was observed in stimulated cells transfected with m2 alone or with m2 plus $G\alpha_{qi5}$ (Fig. 1*B*). To determine the effect of $G\alpha_q$ and $G\alpha_{13}$ on HO-1 expression, we treated stable cell lines expressing the m2 receptor alone (NIH-m2) or in combination with the $G\alpha_{13i5}$ or $G\alpha_{qi5}$ chimeras (NIH-m2-$G_{13i5}$ or NIH-m2-$G_{qi5}$, respectively) (40) with carbachol for 2, 4, and 8 h. After extracting total RNA, levels of HO-1 mRNA at each time point were determined by quantitative PCR. As shown in Fig. 1*C*, all three cell lines had similar basal levels of *ho-1* mRNA. Carbachol induced *ho-1* mRNA levels by 2.5- and 4-fold after 2- and 4-h treatments, respectively, only in NIH-m2-$G_{13i5}$ cells. No increase of *ho-1* mRNA levels was detected after carbachol treatment in NIH-m2 or NIH-m2-$G_{qi5}$ cells. As a control of the activity of the $G_{qi5}$ chimeras, we measured the levels of c-*jun* mRNA levels at 30 min and 1 h after carbachol treatment, and as expected, c-*jun* levels were increased as previously shown (40) (data not shown). Taken together, the data suggested that G proteins of the $G\alpha_{12/13}$ family can induce both transformation and HO-1 expression.

*$G\alpha_{12}$ and $G\alpha_{13}$ Mediate vGPCR-induced HO-1 Expression and Transformation*—The $G\alpha_{12}$ family of $G\alpha$ heterotrimeric G proteins consists of $G\alpha_{12}$ and $G\alpha_{13}$ subunits, and both are potent oncogenes (49). Thus, we studied whether both isoforms were able to activate the *ho-1* promoter. We performed luciferase assay experiments cotransfecting pHO1-Luc, a reporter plasmid with a luciferase cDNA sequence under the control of the *ho-1* promoter, along with increasing concentrations of activated forms of $G\alpha_{12}$ and $G\alpha_{13}$, $Ga_{12}$QL, and $G\alpha_{13}$QL. As shown in Fig. 2*A*, both $G\alpha$ subunits activated pHO1-Luc by severalfold inductions in a manner comparable with vGPCR. To explore whether these subunits mediated vGPCR-induced HO-1 expression, we knocked down $G\alpha_{12}$ and $G\alpha_{13}$ expression in NIH-vGPCR cells, which stably expressed vGPCR and display increased levels of HO-1 (25). We stably transfected them with plasmids carrying shRNA sequences for $G\alpha_{12}$ ($shG_{12}$) and $G\alpha_{13}$ ($shG_{13.1}$ and $shG_{13.2}$) and analyzed protein levels by Western blot. As shown in Fig. 2*B*, individual knocked down expression of $G\alpha_{12}$ or $G\alpha_{13}$ (*first* and *second panels*) strongly reduced the expression of HO-1 (*third panel*). Strikingly, when both isoforms were knocked down simultaneously, the expression of HO-1 was nearly abolished, confirming the important role of these two $G\alpha$ subunits in the pathway that connects vGPCR to HO-1 expression. Equal protein loading in each lane was assessed by detecting $\alpha$-actin in parallel samples. The specificity of $G\alpha_{12}$ and $G\alpha_{13}$ antibodies was confirmed by transfecting HEK-293T cells with equal amounts of $G\alpha_{12}$ and $G\alpha_{13}$, and no crossed reaction was observed (Fig. 2*C*). To verify that the differences in HO-1 expression levels were not due to differences in vGPCR expression levels among the cell lines, the amount of receptor was determined by RT-PCR from extracted total RNA samples. Housekeeping GAPDH mRNA was amplified in parallel as loading control from the same RNA samples.

To determine the role of $G\alpha_{12}$ and $G\alpha_{13}$ in vGPCR-induced transformation and to study the correlation with HO-1 expres-

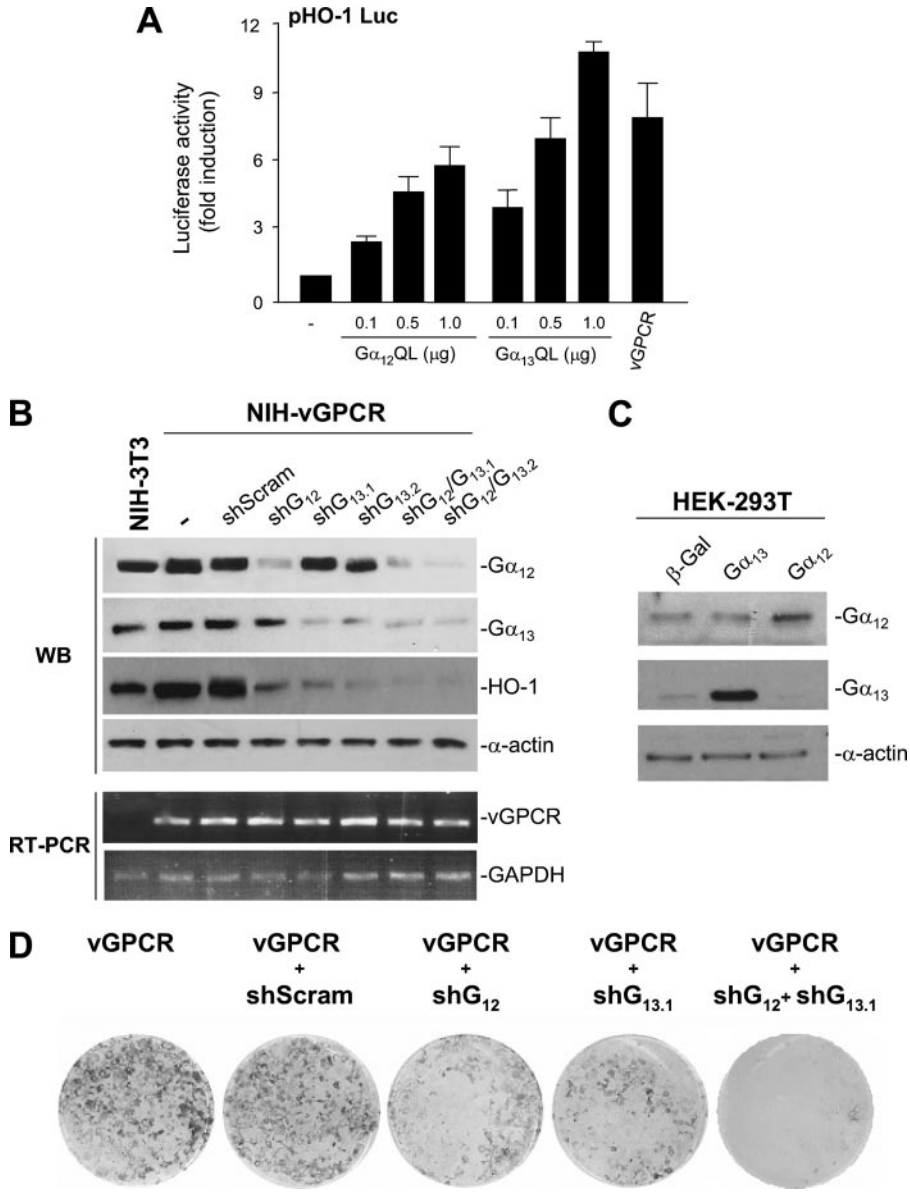


FIGURE 2. **$G\alpha_{12}$ and $G\alpha_{13}$ mediate vGPCR-induced transformation and HO-1 expression.** *A*, NIH-3T3 cells were cotransfected with 10 ng of pHO1-Luc along with 100 ng of pRenilla-Luc and different amounts of pCDNAIII-$G\alpha_{12}$QL and pCEFL-HA-$G\alpha_{13}$QL per well as indicated. The total amount of DNA in each transfection was equally adjusted with pcDNAIII-β-galactosidase. 24 h after transfection and serum starvation, lysates were assayed for luciferase activities. The data represent average Firefly luciferase activity normalized by *Renilla* luciferase activity in each sample ± S.E. from triplicates expressed as -fold induction relative to control from a typical experiment. Similar results were obtained in three additional experiments. *B*, NIH-3T3, NIH-vGPCR, NIH-vGPCR$_{shScram}$, NIH-vGPCR$_{shG12}$, NIH-vGPCR$_{shG13.1}$, NIH-vGPCR$_{shG13.2}$, NIH-vGPCR$_{shG12/G13.1}$, and NIH-vGPCR$_{shG12/G13.2}$ cell lines were serum-starved for 24 h. Lysates were analyzed for HO-1, $G\alpha_{12}$, and $G\alpha_{13}$ and α-actin by Western blot (*WB*) with specific antibodies. Equal amounts or total lysates were loaded in each lane. Parallel samples were analyzed by RT-PCR to detect vGPCR and GAPDH. *C*, HEK-293T cells transfected with pCDNAIII-$G\alpha_{12}$QL and pCEFL-HA-$G\alpha_{13}$QL as indicated. 24 h after transfection, cell lysates from each transfection were analyzed for $G\alpha_{12}$, $G\alpha_{13}$, and α-actin by Western blot with the same antibodies used in *B*. Depicted blots are representative of three independent experiments. *D*, NIH-3T3 cells were transfected using the calcium phosphate technique with 1 μg of pCEFL-AU5-vGPCR and pSshScram, pSshG12, and pSshG13.1, as indicated. After 3 weeks, plates were fixed and stained to score formation of foci. Plates shown are representative of three different experiments.

sion levels, we next carried out focus formation assays transfecting vGPCR alone or in combination with the shRNAs for $G\alpha_{12}$, $G\alpha_{13}$, or both in NIH3T3 fibroblasts. As depicted in Fig. 2*D*, vGPCR-induced transformation was significantly reduced by both shRNAs, whereas knocking down the expression of both subunits had a very pronounced effect as only few foci appeared. Together these results indicate that $G\alpha_{12}$ and $G\alpha_{13}$ participate in the signaling pathway that links vGPCR to HO-1 expression and transformation.

*vGPCR Activates the Small GTPase RhoA*—$G\alpha_{12}$ and $G\alpha_{13}$ activate a family of Rho GTP exchange factors (RhoGEFs) such as PDZRhoGEF and p115RhoGEF, which in turn trigger the activation of the small GTPase RhoA (48–50). These RhoGEFs display a common motif denominated RGS (regulator of G protein signaling) domain (50) through which they bind GTP-bound forms of $G\alpha_{12}$ and $G\alpha_{13}$ (51). Based on this, constructs coding for the RGS domain act as inhibitors of the $G\alpha_{12/13}$ pathways, because they displace the coupling of Gα to endogenous RhoGEFs and consequent RhoA activation (29, 43, 52). Thus, to determine whether the $G\alpha_{12/13}$ pathway was required for vGPCR-induced HO-1 expression, we cotransfected cells with vGPCR and pHO1-Luc with or without an expression vector carrying the RGS domain of p115RhoGEF (p115RGS-D) (29, 52). As shown in Fig. 3*A*, p115RGS-D inhibited vGPCR-induced pHO1-Luc activity by nearly 50% corroborating that $G\alpha_{12/13}$ participate in the pathway connecting vGPCR to HO-1. As p115RGS-D binds $G\alpha_{12/13}$ but not $G\alpha_q$ (52), this construct inhibited the activation of pHO1-Luc induced by $G\alpha_{13}$QL, but as expected and as previously reported, p115RGS-D did not affect the activation of the serum response element (SRE) (pSRE-Luc) induced by $G\alpha_q$QL (Fig. 3, *A* and *B*) (29, 43).

Next, to investigate whether vGPCR was able to activate RhoA, we carried out RhoA activation assays transfecting NIH-3T3 cells with increasing amounts of vGPCR as well as $G\alpha_{13}$QL used as a positive control and representative of the $G\alpha_{12/13}$ family. As expected, $G\alpha_{13}$QL increased the levels of RhoA-GTP as determined by the results of RhoA activation assays (Fig. 3*C*, *top*). The level of GTP-bound RhoA was also increased by different concentrations of vGPCR (Fig. 3*C*, *bottom*). Lysates from cells transfected with an expression vector for the activated form of RhoA, RhoAQL, or cell lysates incu-

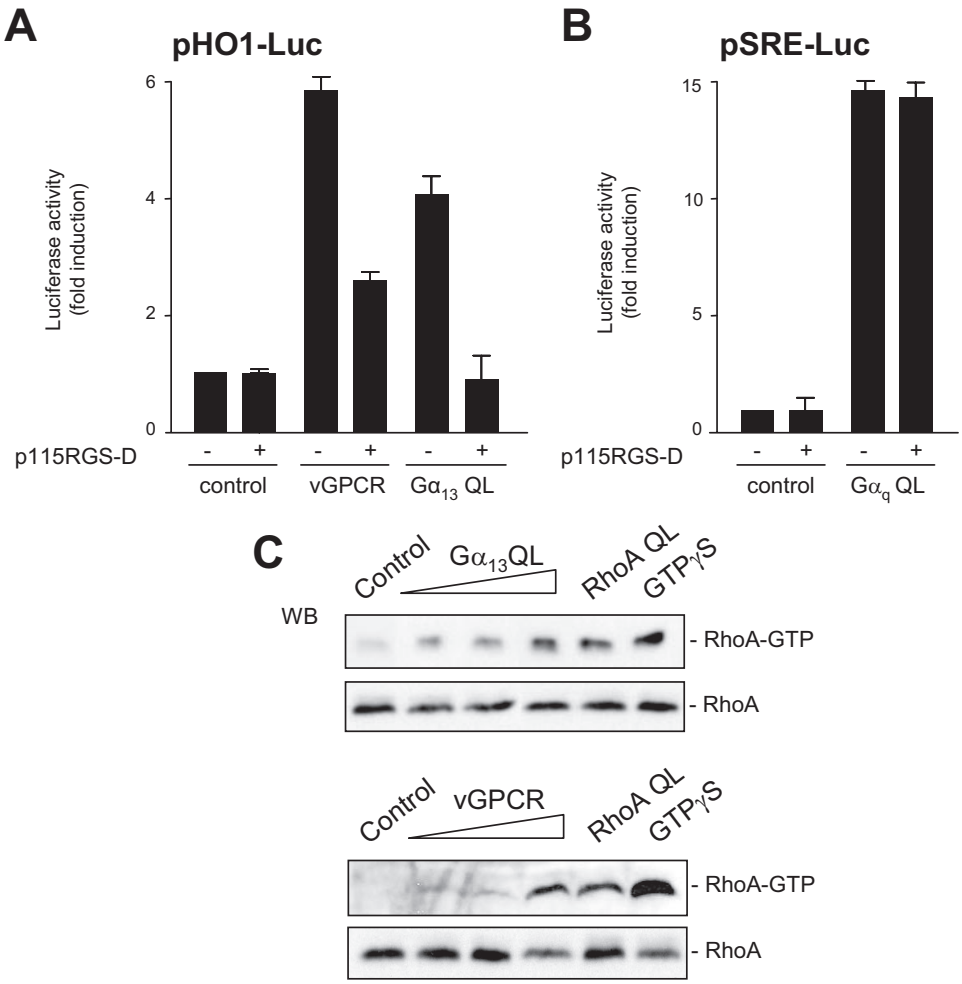


FIGURE 3. **vGPCR activates the small GTPase RhoA.** *A* and *B*, NIH-3T3 cells were cotransfected with 10 ng of pHO1-Luc or 100 $\mu$g of pSRE-Luc along with 100 ng of pRenilla-Luc and 1 $\mu$g of the expression plasmids pcDNAIII-$\beta$-galactosidase (control), 0.1 $\mu$g pCEFL-HA-G$\alpha_{13}$QL, 0.5 $\mu$g of pCEFL-AU5-vGPCR, or 0.1 $\mu$g of pCDNAIII-G$\alpha_q$QL with (+) or without (−) pCEFL-p115RGS-D per well, as indicated. The total amount of plasmid DNA in each transfection was equally adjusted with pcDNAIII-$\beta$-galactosidase. 24 h after transfection and serum starvation, lysates were assayed for luciferase activities. The data represent average firefly luciferase activity normalized by *Renilla* luciferase activity in each sample ± S.E. from triplicates expressed as -fold induction relative to control from a typical experiment. Similar results were obtained in three additional experiments. *C*, NIH-3T3 cells were transfected with pcDNAIII-$\beta$-galactosidase (control), pCEFL-HA-G$\alpha_{13}$QL, pCEFL-AU5-vGPCR, or pCEFL-AU5-RhoAQL as indicated. After 24 h of serum starvation, cells were lysed and incubated with GTP$\gamma$S when indicated. All lysates were incubated with glutathione *S*-transferase-Rhotekin beads and analyzed by Western blot (*WB*) to detect the levels of GTP-bound RhoA (RhoA-GTP) using a RhoA-specific monoclonal antibody. Total RhoA was detected in whole lysates from the same samples. Blots are representative of three independent experiments.

bated with GTP$\gamma$S were used as positive controls. These results confirmed that vGPCR activated the G$\alpha_{12/13}$ downstream effector RhoA and that impairing signaling from G$\alpha_{12/13}$ to RhoA reduces vGPCR-induced *ho-1* promoter activity.

*RhoA Activates HO-1 Expression*—To investigate whether RhoA can induce the activation of the *ho-1* promoter, we performed luciferase assays by transfecting pHO1-Luc with increasing concentrations of a constitutively active mutant of RhoA, RhoAQL (45). As shown in Fig. 4*A*, RhoAQL activated the *ho-1* promoter to an extent comparable with that of the G$\alpha_{12}$, G$\alpha_{13}$, and vGPCR (Fig. 2A). To study if RhoA can activate the expression of the endogenous HO-1 protein, we transfected cells with 1 $\mu$g of RhoAQL as above and measured HO-1 protein levels by Western blot. RhoAQL induced a 4-fold increase in HO-1 protein levels with respect to cells transfected with $\beta$-galactosidase (control). Lysates from cells transfected with pCEFL-HA-HO-1 were analyzed in parallel to show the specificity of the HO-1 antibody (Fig. 4*B*). The upper band corresponded to transfected HA-HO-1, and the lower corresponded to endogenous protein. As expected, cells transfected with HO-1 displayed increased levels of endogenous protein, most likely due to a feedback mechanism, where the signaling pathways activated as a consequence of the HO-1 enzymatic activity further impinge on the *ho-1* promoter (25). Similar results were seen in indirect immunofluorescence assays, where cells transfected with AU5-tagged RhoAQL (*green*) showed increased levels of endogenous HO-1 (*red*) (Fig. 4*C*, *right*), whereas control cells expressing the GFP (*green*) displayed only basal levels of HO-1 protein (*red*, *left*). The presence of cells present in the visualized fields was evidenced by staining nuclei with DAPI (bottom).

To determine whether activation of endogenous RhoA resulted in *ho-1* promoter activation and HO-1 expression, we transfected cells with p115RhoGEF or PDZRhoGEF (47) and performed luciferase and immunofluorescence assays. Both RhoGEFs strongly induced the activity of pHO1-Luc and endogenous HO-1 expression (data not shown). Altogether, these results showed that activated RhoA was able *per se* to induce *ho-1* promoter activity and HO-1 protein expression.

*RhoA Mediates vGPCR-induced HO-1 Expression*—To study the involvement of RhoA in the signaling pathway linking vGPCR to the *ho-1* promoter, we used several approaches. First, we used a negative dominant form of RhoA, RhoN19, and the C3 toxin inhibitor from *Clostridium botulinum*, which selectively induces the *N*-ADP-ribosylation of Rho proteins and inhibits the activation of Rho-controlled signaling pathways (40). Luciferase assays were carried out cotransfecting pHO1-Luc with expression vectors for vGPCR or G$\alpha_{13}$QL alone or together with RhoN19 or C3. RhoN19 reduced vGPCR and G$\alpha_{13}$-induced activation of pHO1-Luc by 45–50% with respect to the control, whereas C3 had a more dramatic effect inhibiting pHO1-Luc activation by almost 90% in both cases (Fig. 5*A*). Under identical experimental conditions, RhoN19 and C3 did not affect Rac1QL-induced pNF$\kappa$B-Luc activity (a reporter plasmid with the luciferase gene

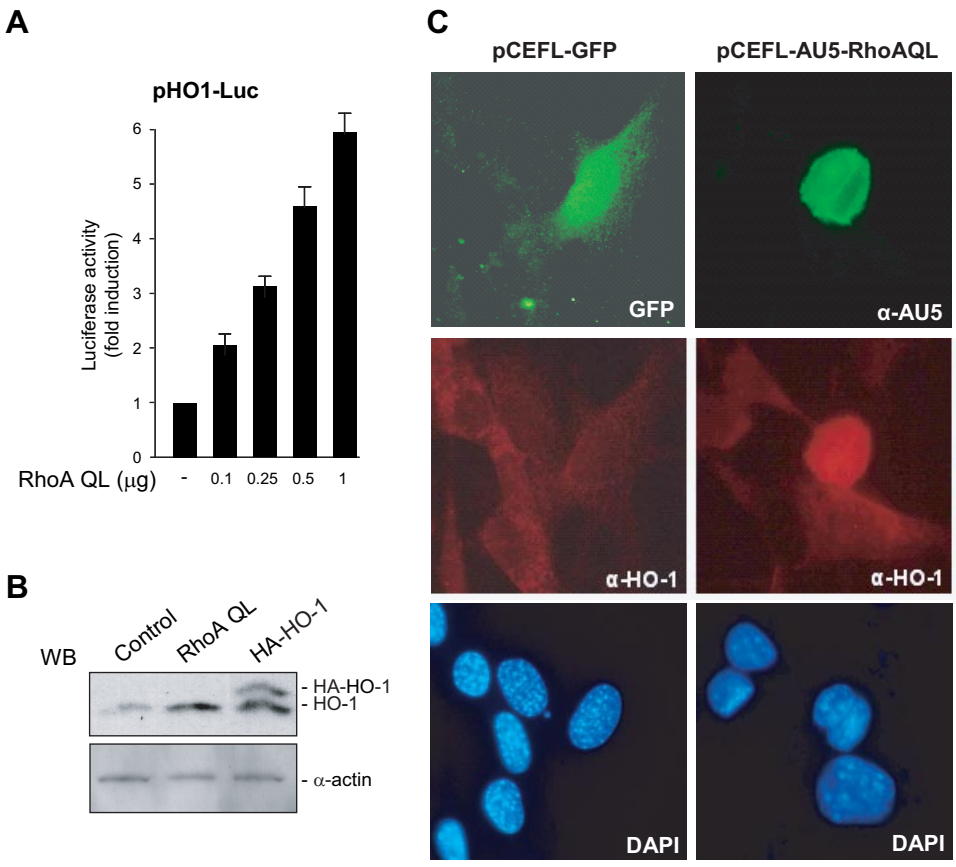


FIGURE 4. **RhoA activates HO-1 expression.** *A*, NIH-3T3 cells were cotransfected with 10 ng of pHO1-Luc along with 100 ng of pRenilla-Luc and different amounts of pCEFL-AU5-RhoAQL per well as indicated. The total amount of DNA in each transfection was equally adjusted with pcDNAIII-β-galactosidase. 24 h after transfection and serum starvation, lysates were assayed for luciferase activities. The data represent average firefly luciferase activity normalized by *Renilla* luciferase activity in each sample ± S.E. from triplicates expressed as -fold induction relative to control from a typical experiment. Similar results were obtained in three additional experiments. *B*, NIH-3T3 cells were transiently transfected with 1 μg of pcDNAIII-β-galactosidase (control), pCEFL-AU5-RhoAQL, or pCEFL-HA-HO-1 and serum-starved for 24 h. Equal amounts of total cell lysates were loaded in each lane and analyzed by Western blot (*WB*) for HO-1 and α-actin with specific monoclonal antibodies. *C*, NIH-3T3 cells were seeded on coverslips, transfected with pCEFL-AU5-RhoAQL or pCEFL-GFP, serum-starved, and analyzed by immunofluorescence to detect GFP (*green*), AU5-RhoAQL (*green*), and HO-1 (*red*) expression with anti-AU5 and anti-HO-1 antibodies. Nuclei were stained with DAPI. *Images* are representative of more than 100 different fields.

driven by five tandem copies of NFκB response elements) (53), indicating their specificity as Rho inhibitors (Fig. 5*B*).

We next knocked down the expression of RhoA by using specific small hairpin RNAs (shRNAs). We first inserted two different RhoA-specific shRNAs (shRho1 and shRho2) and a scramble shRNA (shScram) into the pSilencer vector and transiently transfected them in HEK-293T along with RhoAQL. Both shRho1 and -2 strongly inhibited RhoA expression, whereas shScram had no significant effect (data not shown). Next, we transfected NIH-vGPCR cells with shRho1 or shRho2 (NIH-vGPCR$_{shRho1}$ and NIH-vGPCR$_{shRho2}$, respectively) along with pCEP4. After antibiotic selection and as judged by Western blotting assays, both cell lines presented almost undetectable levels of RhoA when compared with parental NIH-vGPCR cells and even NIH-3T3 cells, the inhibition being stronger in NIH-vGPCR$_{shRho2}$ (Fig. 5*C*, *top*). To determine the specificity of shRho1 and shRho2, the same cell lysates used above were assayed to measure HO-1 and α-actin (control) levels. As expected, reduced levels of RhoA correlated with reduced levels of HO-1 (Fig. 5*C*, *middle*), whereas no changes were observed in the α-actin levels. To corroborate that this inhibition was not due to reduced vGPCR expression or a secondary effect on general transcription, total RNA was isolated from parallel samples, and mRNA levels of vGPCR and GAPDH were assayed by semi-quantitative RT-PCR (25). Fig. 5*C* (*bottom*) shows that NIH-vGPCR, NIH-vGPCR$_{shRho1}$, and NIH-vGPCR$_{shRho2}$ cells expressed equal amounts of viral receptor, whereas no expression was detected in NIH-3T3. GAPDH levels were nearly identical in all four cell lines.

Since activation of RhoA induces stress fiber formation (30) and a previous study shows that vGPCR induces similar cytoskeleton morphology in NIH-3T3 cells (29), we investigated whether inhibition of RhoA affected vGPCR-induced stress fiber formation in NIH-vGPCR$_{shRho2}$, where RhoA levels where nearly abolished. Indeed, as depicted in Fig. 5*D*, phalloidin-stained actin fibers observed in NIH-vGPCR cells across the cytoplasm were unnoticed in NIH-vGPCR$_{shRho2}$, thus confirming the inhibition of RhoA expression and its downstream effects in this cell line. Together, these data indicated that RhoA is involved in vGPCR-induced HO-1 expression.

*Targeted Knockdown RhoA Expression Impairs vGPCR-induced Cell Proliferation, Survival, and Tumorigenesis*—Overexpression of vGPCR increases cell proliferation and reduces serum deprivation-induced apoptosis (25, 54). To investigate whether inhibition of RhoA impairs vGPCR-induced cell proliferation and survival, we performed [$^3$H]thymidine incorporation assays and propidium iodide staining, respectively. Indeed, NIH-vGPCR$_{shRho2}$ cells showed a 40% reduction on [$^3$H]thymidine incorporation, and nearly a 46% increase in the number of apoptotic cells after 48-h serum starvation when compared with NIH-vGPCR (data not shown). To determine whether RhoA was involved in vGPCR-induced cell transformation and tumorigenesis, we seeded 5000 NIH-vGPCR, NIH-vGPCR$_{shRho2}$, or NIH-3T3c (control) cells onto a 50% confluent monolayer of NIH-3T3 cells and cultured them for 2–3 weeks until foci were detected. As shown in Fig. 6*A*, NIH-vGPCR cells induced the formation of numerous foci, whereas a very limited number was formed by NIH-vGPCR$_{shRho2}$ cells, despite the fact that both cell lines expressed the same amount of vGPCR (Fig.

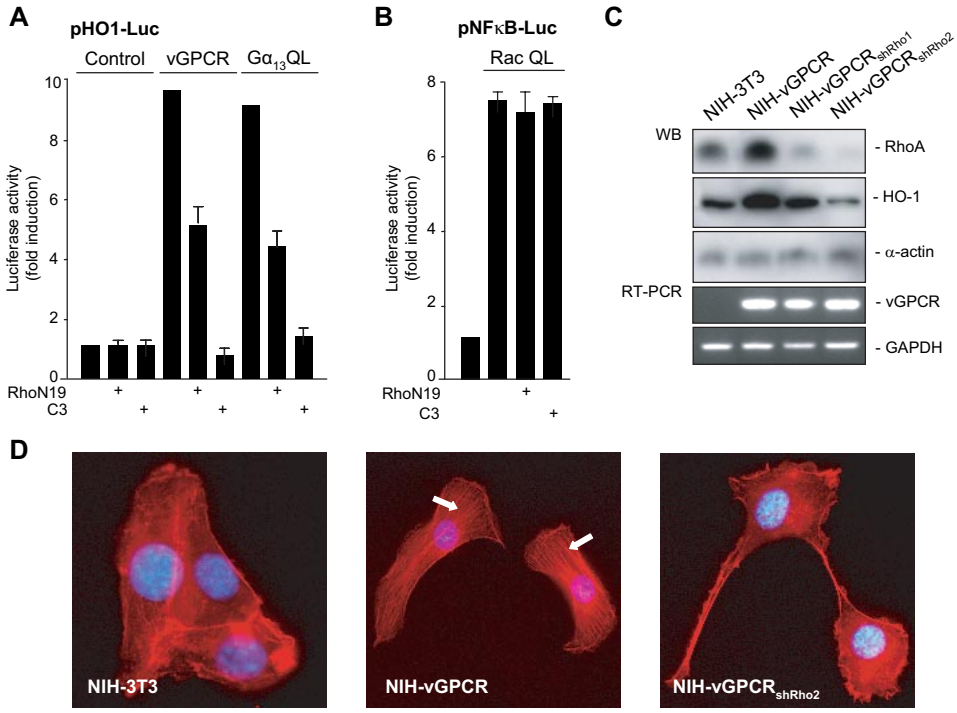


FIGURE 5. **RhoA mediates vGPCR-induced HO-1 expression.** *A* and *B*, NIH-3T3 cells were cotransfected with 10 ng of pHO1-Luc or 100 μg of pNFκB-Luc along with 100 ng of pRenilla-Luc and 1 μg of pCEFL-HA-Gα$_{13}$QL, pCEFL-AU5-vGPCR, pCEFL-RhoN19, pEF-C3, or pCEFL-AU5-RacQL per well as indicated. The total amount of plasmid DNA in each transfection was equally adjusted with pcDNAIII-β-galactosidase. 24 h after transfection and serum starvation, lysates were assayed for luciferase activities. The data represent average firefly luciferase activity normalized by *Renilla* luciferase activity in each sample ± S.E. from triplicates and are expressed as -fold induction relative to control from a typical experiment. Similar results were obtained in three additional experiments. *C*, NIH-3T3, NIH-vGPCR, NIH-vGPCR$_{shRho1}$, and NIH-vGPCR$_{shRho2}$ cells were serum-starved for 24 h. Lysates were analyzed for HO-1, RhoA, and α-actin by Western blot (*WB*) with specific monoclonal antibodies. Equal amounts or total lysates were loaded in each lane. Parallel samples were analyzed by RT-PCR to amplify vGPCR and GAPDH. *D*, NIH-3T3, NIH-vGPCR, and NIH-vGPCR$_{shRho2}$ cells were seeded on coverslips, serum-starved, incubated with phalloidin, and analyzed by immunofluorescence to detect stress fibers. Nuclei were stained with DAPI. *Images* are representative of more than 100 different fields. The *white arrows* indicate the presence of stress fibers.

5*C*). As expected, no foci were originated by NIH-3T3c cells used as a control. Second, we investigated whether inhibition of RhoA had the same effect on vGPCR-induced tumor formation using a murine allograft tumor model (23, 25). 1 × 10$^6$ NIH-vGPCR cells (Group 1) or NIH-vGCPR$_{shRho2}$ cells (Group 2) were injected in the right flank of athymic nude mice. One week after the injection, tumors of around 5 mm$^3$ were apparent in all animals in the first group, and after 21 days, tumors grew to a volume of 891 ± 230 mm$^3$ (mean ± S.E.). Strikingly, and although both cell lines displayed the same levels of vGPCR (Fig. 5*B*), only one animal in the second group developed a tumor that after 21 days only reached an approximate volume of 10 mm$^3$ (Fig. 6*B*). Given this remarkable and significant difference ($p \leq 0.05$), these results strongly suggested that RhoA is a key mediator of vGPCR-induced tumorigenesis.

*HO-1 Mediates RhoA-induced Transformation*—RhoA mediates the effect of several transforming GPCRs (39, 40, 55), and the constitutively activated form can itself act as an oncogene when it is overexpressed in cultured cells (38, 39). To investigate whether HO-1 participated in the transforming effect of the RhoA pathway we used different approaches. We prepared a stable cell line expressing AU5-tagged RhoAQL and further transfected it with the empty shRNA vector pSilencer or with the same vector carrying shRNA sequences specific for HO-1, pSshRNAHO-1 (25), to produce NIH-RhoAQL and NIH-RhoAQL$_{shHO-1}$ cells, respectively. As depicted in Fig. 7*A*, Western blot analysis showed that HO-1 levels were induced by 4-fold in NIH-RhoA cells with respect to normal NIH-3T3, confirming that RhoA induces HO-1 expression (Fig. 4, *B* and *C*), whereas HO-1 expression was dramatically reduced in NIH-RhoAQL$_{shHO-1}$, with respect to NIH-RhoAQL and even NIH-3T3 cells. AU5-RhoAQL levels were identical in NIH-RhoAQL and NIH-RhoAQL$_{shHO-1}$ (Fig. 7*A*, *middle*). α-Actin levels were identical in all cell lines, indicating that the shRNA HO-1 did not target this mRNA used as a control (Fig. 7*A*, *bottom*).

To measure whether RhoA activation increased cell proliferation and survival, two of the key events in the process of transformation, we carried out DNA synthesis and *in vitro* apoptosis assays. As evidenced by [$^3$H]thymidine incorporation, NIH-RhoAQL cells displayed a 2.5-fold higher proliferation rate when compared with parental NIH-3T3 cells (Fig. 7*B*). Similarly, cell survival was increased in NIH-RhoAQL cells as evidenced by a nearly 60% reduction in the population of apoptotic cells compared with NIH-3T3 (Fig. 7*C*). Knocked down HO-1 expression in shRNANIH-RhoAQL$_{shHO-1}$ cells resulted in almost 36% reduction in [$^3$H]thymidine incorporation assays and in a nearly 40% increase in the number of apoptotic cells with respect to NIH-RhoAQL (Fig. 7, *B* and *C*), although both cell lines expressed comparable amounts of RhoAQL (Fig. 7*A*). In line with these observations, inhibition of HO-1 activity in NIH-RhoAQL cells by treatment with 100 μM SnPP, a chelate of tin with the porphyrin ring that binds HO-1 and specifically abolishes its activity (56), reduced DNA synthesis and increased the number of apoptotic cells with respect to vehicle-treated cells (Fig. 7, *B* and C). These results showed that either knocking down HO-1 expression or blocking its enzymatic activity reduced RhoAQL-induced DNA synthesis and increased apoptosis, suggesting that HO-1 mediated at least in part the effect of RhoA on cell proliferation and survival.

To determine whether HO-1 participated in the process of RhoA-induced transformation, we next performed focus formation assays by transfecting NIH-3T3 cells with expression plasmids coding for RhoAQL and the RhoA upstream activators Gα$_{13}$QL and PDZRhoGEF. We knocked down HO-1 expression by cotransfecting cells with pSshRNAHO-1 or inhibited HO-1 activity by treating cells with SnPP. As shown in

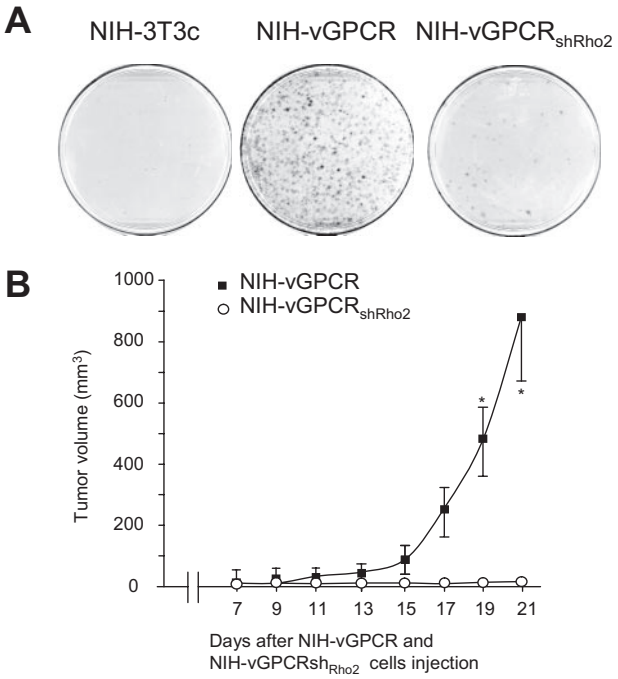


FIGURE 6. **Targeted knockdown RhoA expression impairs vGPCR-induced transformation and tumorigenesis.** *A*, $5 \times 10^4$ NIH-3T3c (control), NIH-vGPCR, and NIH-vGPCR$_{shRho2}$ cells were cultured on a monolayer of NIH-3T3 cells as indicated. After 3 weeks, plates were fixed and stained to score formation of foci. Representative plates from three different experiments are shown. *B*, $1 \times 10^6$ NIH-vGPCR or NIH-vGPCR$_{shRho2}$ cells were injected in the right flank of two groups of five nude mice each. Tumor volumes were measured every other day. Data are mean volume ± S.E. from $n = 5$ in each group. Mean values for each group in a given day were compared using the *t* test. *, $p \leq 0.05$.

Fig. 7*D* (*top*), G$\alpha_{13}$QL, PDZRhoGEF, and RhoAQL induced the appearance of foci with a vGPCR-like morphology, whereas both the transfection with shRNAHO-1 (*middle*) and the treatment with SnPP (*bottom*) dramatically reduced the amount of foci. In all, these results suggested that HO-1 mediated RhoA-elicited cell survival and proliferation as well as cell transformation induced by molecular components of the RhoA pathway.

*HO-1 Mediates vGPCR and RhoA-induced VEGF-A Expression and Secretion*—Previous studies showed that vGPCR induces VEGF-A expression and that this is an essential process in tumor development (57, 58). We and others have previously observed that HO-1 overexpression induces VEGF-A expression (10, 25, 59) and that inhibition of HO-1 activity with SnPP blocks vGPCR-induced VEGF-A expression (25). To study if molecular components of the RhoA signaling pathway can induce VEGF-A expression, NIH-3T3 cells were transfected with a luciferase expression plasmid under the control of the *VEGF-A* promoter (pVEGF-Luc) along with G$\alpha_{13}$QL, PDZRhoGEF, or RhoAQL. All of these proteins activated pVEGF-Luc, and this induction was significantly reduced when cells were cotransfected with pshRNAHO-1 or treated with SnPP (Fig. 8*A*). Therefore, our data showed that activation of the RhoA signaling pathway leads to enhanced VEGF-A expression and that HO-1 links, at least partially, these two events.

Since secretion of VEGF-A and its paracrine effect are an important step in transformation of adjacent cells and tumor development (57), we measured VEGF-A secretion from NIH-RhoAQL, NIH-RhoAQL$_{shHO-1}$, and NIH-vGPCR$_{shRho2}$ cells by a VEGF-A enzyme-linked immunosorbent assay using NIH-vGPCR as a positive control. Results show that NIH-RhoAQL cells secreted a VEGF-A level comparable with those secreted by NIH-vGPCR cells (nearly 6–7-fold induction with respect to NIH-3T3 cells). VEGF-A secretion in NIH-vGPCR was reduced by almost 80% by treatment with 100 $\mu$M SnPP and by 60% in NIH-vGPCR$_{shRho2}$ cells. Similarly, SnPP treatment reduced VEGF-A secretion by 57% in NIH-RhoAQL cells, whereas it was reduced by 50% in NIH-RhoAQL$_{shHO-1}$ cells when compared with untreated NIH-RhoAQL (Fig. 8*B*). These data indicated that RhoA and HO-1 participated in vGPCR-induced VEGF-A expression and secretion.

*HO-1 Participates in RhoA-induced Tumorigenesis*—RhoA has oncogenic potential, and like HO-1 (8, 13, 15, 60, 61), it is overexpressed in several types of cancer (62–65). To determine whether there is a functional link between RhoA-induced tumorigenesis and HO-1 expression, $1 \times 10^6$ NIH-RhoAQL cells were injected in the right flank of 10 athymic nude mice. Tumors were noticeable in all animals after 4–6 days, and at that point, mice were split in two groups. One group was injected every other day with vehicle (0.2 N NaOH in 1× PBS, pH 7.4), and the other was injected with 10 $\mu$mol/kg of body weight of SnPP dissolved in 0.2 N NaOH in 1× PBS, pH 7.4. Both treatments were administered in parallel and during a period of 21 days. As shown in Fig. 9*A*, treatment with SnPP for 21 days inhibited tumor growth by an average of 70% ($p \leq 0.05$). SnPP did not induce evident macroscopic secondary effects, since no internal organ changes either in morphology or size were observed in SnPP-treated animals with respect to controls (data not shown), except for a light red coloration of the skin most likely due to the accumulation of SnPP in this organ as previously reported (25). Similarly, vehicle- and SnPP-treated animals showed no differences in body weight and general behavior, which indicates the lack of apparent toxic side effects of the SnPP during the length of the experiment. Histological examination of liver and skin sections showed the absence of tissue necrosis in both groups (data not shown) as previously reported (25).

To investigate the levels of AU5-RhoA, HO-1, and VEGF-A in the tumors, mRNA from three control and three treated tumors was extracted, and semiquantitative RT-PCRs were performed. As depicted in Fig. 9*B*, AU5-tagged RhoA was expressed in comparable amounts in tumors from both groups of animals. HO-1 expression was detected in tumors induced by RhoA, and its expression was further increased by SnPP treatment. As previously described, SnPP is a competitive inhibitor that regulates heme oxygenase by a dual mechanism. On one hand, it enhances the activity of the *ho-1* promoter, but on the other hand, it potently inhibits the enzyme at the catalytic site by acting as a competitive substrate for heme. Inhibition of heme oxygenase by SnPP is so pronounced that, despite the marked increase in the synthesis of new enzyme, suppression of heme oxidation is the prevailing biological effect (56). In line with this, we have previously shown that in vGPCR tumors from SnPP-treated animals, HO-1 enzymatic activity is completely abolished, although HO-1 expression is increased when compared with tumors from control animals (25). On the con-

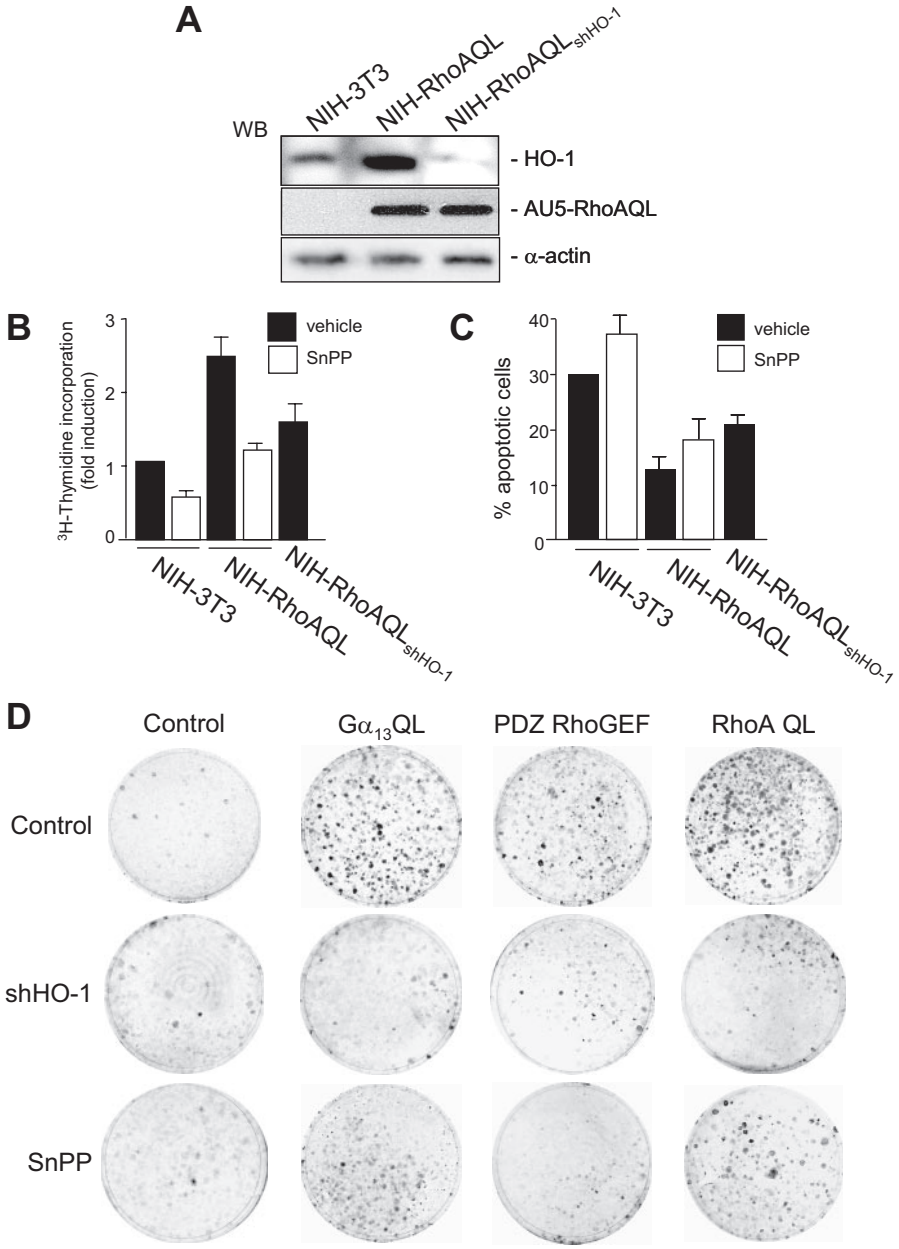


FIGURE 7. **HO-1 mediates RhoA-induced transformation.** *A*, NIH-3T3, NIH-RhoA, and NIH-RhoA$_{shHO-1}$ cells were serum-starved for 24 h. Equal amounts of total lysates were loaded in each lane and analyzed for HO-1, AU5-RhoAQL, and α-actin by Western blot (*WB*) with specific monoclonal antibodies. *B*, NIH-3T3, NIH-RhoA, and NIH-RhoA$_{shHO-1}$ cells were serum-starved, treated with 100 μM SnPP or vehicle for 24 h, and incubated with [$^3$H]thymidine. Results are the average of incorporated radioactivity normalized by total protein ± S.E. from triplicates and expressed as -fold induction relative to control NIH-3T3, whose value was taken as 1. Similar results were obtained in three independent experiments. *C*, NIH-3T3, NIH-RhoAQL, and NIH-RhoAQL$_{shHO-1}$ cells were serum-starved, treated with 100 μM SnPP or vehicle for 24 h, and stained with propidium iodide. Cells were then analyzed by flow cytometry, and the sub-$G_0/G_1$ fraction was used as a measure of the apoptotic percentage. Results shown are representative of triplicate experiments. *D*, NIH-3T3 cells were transfected by the calcium phosphate technique with 1 μg of pcDNAIII-β-galactosidase (control), pCEFL-HA-Gα$_{13}$QL, pCEFL-AU1-PDZRhoGEF, or pCEFL-AU5-RhoAQL as indicated. Cells were cotransfected with pSshRNAHO-1 or treated with 100 μM SnPP as depicted and cultured in 5% calf serum. After 3 weeks, plates were fixed and stained to score formation of foci. Plates shown are representative of three different experiments.

Immunohistochemistry of RhoAQL-induced tumors showed high expression of HO-1, which, as explained above, was further increased in tumors from SnPP-treated animals (Fig. 9*C*, *top*). Conversely, VEGF-A expression was high in tumors from vehicle-treated animals and significantly reduced in tumors from those treated with SnPP (Fig. 9*C*, *middle*). Hematoxylin-eosin staining showed that RhoAQL-induced tumors display cells with a spindle-shaped morphology characteristic of the human Kaposi sarcoma lesions and similar to those found in vGPCR-induced tumors (23, 25). This phenotype was altered in SnPP-treated tumors, since the cell population was less dense, and cells were more rounded (Fig. 9*C*, *bottom*). Nearly identical results were obtained when tumors were induced by NIH-Gα$_{13}$QL-expressing cells. SnPP reduced tumor growth by 60% and strongly inhibited tumor VEGF-A expression (data not shown). These data strongly suggest that HO-1 activity participates in the tumorigenic potential of the RhoA pathway.

Taking advantage of the NIH-RhoAQL and NIH-RhoA$_{shHO-1}$ cell lines characterized and described above (Fig. 7*A*), we injected $1 \times 10^6$ cells of each population into the right flank of two groups of five nude mice. Although both cells showed identical levels of AU5-RhoAQL (Fig. 7*A*), tumor growth was reduced by 80% in NIH-RhoA$_{shHO-1}$ cell-bearing mice ($V = 247 \pm 121$ mm$^3$) with respect to tumors induced by NIH-RhoA cells ($V = 1289 \pm 646$ mm$^3$) ($p \leq 0.05$) (Fig. 9*D*). These results robustly indicate that HO-1 plays an important role as an intermediate molecule in the route connecting RhoA to tumorigenesis.

## DISCUSSION

We have recently demonstrated the important role of HO-1, an enzyme expressed in human KS lesions (15), in vGPCR-induced VEGF-A expression and tumorigenesis as well as the use of the HO-1 inhibitor SnPP as a potential tumor growth inhibitor (25). In this study, we identified the Gα$_{12/13}$/RhoA signaling route as a key component

trary, VEGF-A expression in RhoAQL-induced tumors was strongly inhibited by SnPP treatment, as previously seen in vGPCR-induced tumors obtained from SnPP-treated animals (25). GAPDH amplification was used as a loading control (Fig. 9*B*, *bottom*).

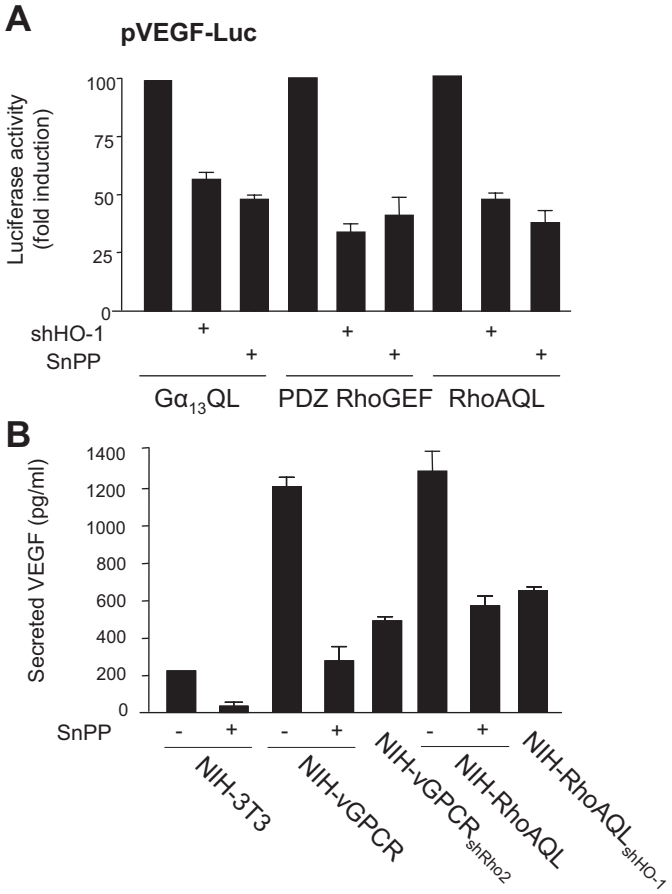


FIGURE 8. **HO-1 mediates vGPCR and RhoA-induced *VEGF* promoter and VEGF secretion.** *A*, NIH-3T3 cells were cotransfected with 10 ng of pVEGF-Luc along with 100 ng of pRenilla-Luc and 1 $\mu$g of pCEFL-HA-G$\alpha_{13}$QL, pCFEL-AU1-PDZRhoGEF, or pCEFL-RhoAQL per well. Cells were cotransfected with pSshRNAHO-1 or treated with 100 $\mu$M SnPP (+). The total amount of plasmid DNA in each transfection was equally adjusted with pcDNAIII-$\beta$-galactosidase. 24 h after transfection and serum starvation, lysates were assayed for luciferase activities. The data represent average firefly luciferase activity normalized by *Renilla* luciferase activity in each sample ± S.E. from triplicates expressed as a percentage of induction relative to the maximal activation induced by G$\alpha_{13}$QL, PDZRhoGEF, or RhoAQL taken as 100%. Similar results were obtained in three additional experiments. *B*, VEGF was detected by an enzyme-linked immunosorbent assay from samples of conditioned media from overnight growth of 24-h starved NIH-3T3, NIH-vGPCR, NIH-RhoA, NIH-vGPCR$_{shRho2}$, and NIH-RhoA$_{shHO-1}$ cells treated with vehicle (−) or SnPP (+). Results are the average of secreted VEGF normalized by total protein ± S.E. in triplicate samples and expressed as pg/ml. Similar results were obtained in two independent experiments.

that connects vGPCR to HO-1 expression and as part of the intricate signaling network by which the receptor induces transformation.

Although few recent studies show that HO-1 can be induced by GPCRs, such as $\beta$1-adrenoreceptors, melanocortin, angiotensin, non-*N*-methyl-D-aspartate, and metabotropic receptors (5, 32, 34), to the best of our knowledge, this is the first study describing the nature of the G$\alpha$ subunits connecting a GPCR with the *ho-1* promoter. vGPCR couples functionally to G$\alpha_q$, G$\alpha_i$, and G$\alpha_{12}$ families of G$\alpha$ proteins and distinctly transduces the signal to several pathways (19, 27, 44). Here, we show that the induction of HO-1 expression by G$\alpha_{12/13}$ correlated with the ability of this family of subunits to induce transformation. Indeed, only receptor-activated G$\alpha_{13i5}$ chimeras induced HO-1 and the appearance of foci, whereas carbachol-activated Gq$_{i5}$ chimeras induced neither HO-1 nor the appearance of foci. The fact that the p115RGS domain (37) blocked vGPCR-induced activation of the *ho-1* promoter without affecting G$\alpha_q$-induced pSRE-Luc activity (Fig. 3, *A* and *B*) indicates that G$\alpha_{12}$ and G$\alpha_{13}$ mediate at least in part the connection between vGPCR and HO-1 expression. Although vGPCR utilizes several G$\alpha$ subunits and their downstream effectors to induce transformation, our data indicate that the induction of HO-1 expression is most likely mediated by the G$\alpha_{12/13}$ family.

The small GTPase RhoA acts downstream of several G$\alpha_{12}$-coupled and G$\alpha_{13}$-coupled receptors, such as the thrombin receptor PAR-1 and LPA receptor, respectively, by promoting the expression of protooncogenes (38, 40). RhoA is highly overexpressed in several cancers, such as gastric carcinoma and pancreatic, colorectal, lung, and breast tumors (62–65), but its role in vGPCR-induced tumorigenesis has not yet been clearly established. Instead, it is known that vGPCR activates the small GTPases Rac and Cdc42 and that Rac mediates vGPCR-induced activation of the NF$\kappa$B transcription factor, thus up-regulating the secretion of critical KS cytokines and ultimately paracrine tumorigenesis (28, 31). Recent studies indicate a critical role for Rac1 and the phosphatidylinositol 3-kinase/AKT pathways in vGPCR-induced NF$\kappa$B activation (31, 66, 67) in endothelial cells, but others suggest that in primary effusion lymphoma cells, NF$\kappa$B activation by vGPCR is not substantially mediated by this pathway (27). Instead, a different study shows that vGPCR-induced NF$\kappa$B activation and interleukin-8 secretion are mediated by the RhoA pathway (29). Interestingly, the direct activation of RhoA by the viral receptor has not yet been demonstrated. In this study, we show that vGPCR induces the GTP loading and activation of RhoA and that targeted knockdown of RhoA expression dramatically impaired vGPCR-induced transformation and tumorigenesis. Moreover, the sole expression of activated RhoA induces cell survival and proliferation to levels comparable with those induced by vGPCR and also provokes a remarkable activation of the *ho-1* promoter and increase of HO-1 protein levels. Conversely, the impairment of endogenous RhoA activity blocks vGPCR-induced ho-1 promoter activity. It is noteworthy that activated Rac1 (Rac1QL) induced slightly the *ho-1* promoter (pHO1-Luc), but a dominant negative Rac1, Rac1 N17 (73), failed to inhibit vGPCR-induced pHO1-Luc activity (data not show).

Although more refined approaches are needed to establish the effect of Rac on HO-1 activation, our results indicate that the G$\alpha_{12/13}$/RhoA axis plays an important role in activating HO-1 expression. In line with this, both G$\alpha_{13}$QL- and RhoAQL-induced tumors display the characteristic spindle cells present in vGPCR-induced tumor and in human KS lesions. Like vGPCR-induced tumors, G$\alpha_{13}$QL- and RhoAQL-induced tumors showed elevated HO-1 mRNA. Moreover, knockdown of HO-1 expression by shRNA in RhoAQL-expressing cells strongly reduced their tumor potential. This indicates that HO-1 is a component of the v-GPCR-activated G$\alpha_{12/13}$/RhoA signaling pathway that leads to tumorigenesis.

From a therapeutic point of view and using a pharmacological approach, it is more striking that the chronic administration of the HO-1 inhibitor SnPP to mice remarkably reduces RhoA-

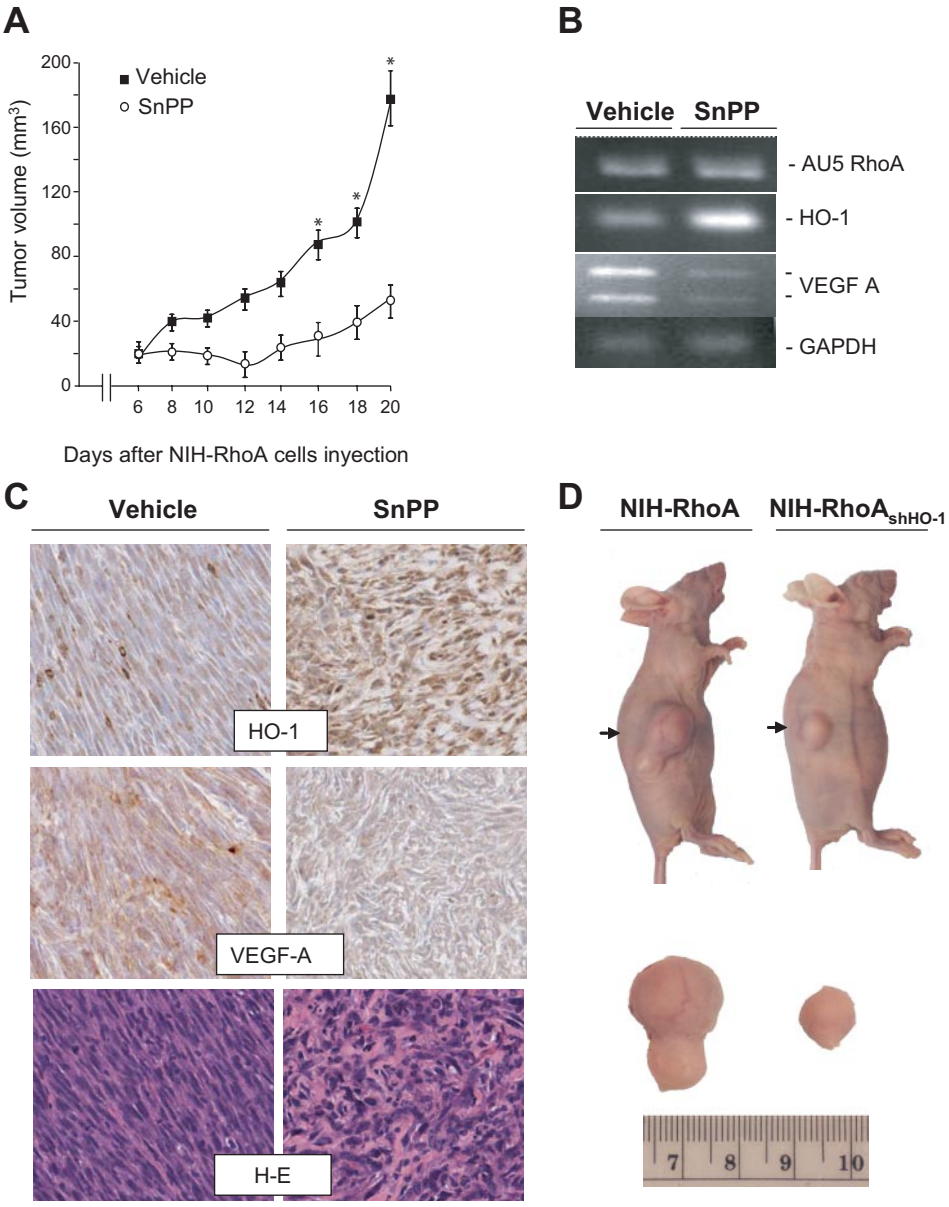


FIGURE 9. **HO-1 participates in RhoA-induced tumorigenesis.** *A*, $1 \times 10^6$ NIH-RhoAQL cells were injected in the right flank of 10 nude mice. Six days after cell injection animals were separated in two groups (five mice each) and treated with vehicle or 10 $\mu$mol/kg of body weight of SnPP in 0.1 N NaOH in PBS, pH 7.4, injected subcutaneously near the tumor area every other day. Tumor volumes were also measured every other day. Data are mean volume ± S.E. from $n = 5$ in each group, $p \leq 0.05$. *B*, expression of AU5-RhoA, HO-1, VEGF-A, and GAPDH mRNA in NIH-RhoAQL-induced tumors from vehicle and SnPP-treated mice was detected by RT-PCR with specific oligonucleotides. Bands shown correspond to ethidium bromide staining of PCR products and are representative of three different tumors analyzed per group. *C*, tumor tissue sections from vehicle and SnPP-treated mice were stained with antibodies anti-HO-1 or VEGF and with hematoxylin-eosyn (*H-E*). *D*, $1 \times 10^6$ NIH-RhoAQL or NIH-RhoAQL$_{shHO-1}$ cells were injected in the right flank of two groups of five nude mice each. The figure shows representative tumor-bearing animals from each group and the corresponding surgically removed tumors 21 days after cell injections (*rule bar* in cm).

induced tumor growth by 70%. This result is comparable with that previously observed in mice bearing vGPCR-induced tumors and treated under the same conditions, where SnPP reduced tumor growth by nearly 80% (25). SnPP is a chelate of tin with the porphyrin ring and has proven to be one of the most efficient inhibitors of HO-1 both *in vitro* and *in vivo* (68–71), and we have shown that HO-1 activity is completely abolished in vGPCR-induced tumors from mice treated with SnPP (25). Moreover, the histological analysis of the tumors shows that treatment with SnPP reverted the spindle-like shape phenotype observed in tumors from untreated animals in favor of tumors with less cell density and scarce, much less evident spindle cells. SnPP has been extensively used *in vivo* to treat several pathologies (72–74) and assayed in clinical trials with newborns to successfully block the progression of postnatal hyperbilirubinemia by blocking heme degradation to bilirubin without significant short or long term side effects in the patients (75). Similarly, the zinc protoporphyrin, another potent HO-1 inhibitor, has an antineoplastic effect in rats and mice bearing tumors derived from hepatoma and human colon cancer cells (9, 76) and also reduces vGPCR-induced tumor growth by 80% (data not shown). Recent evidence shows that HO-1 is overexpressed in pancreatic, gastric, lung, and renal cancer, myeloid leukemia, melanoma, glioma, tongue, thyroid, and hepatocarcinomas (8, 12, 13, 60, 61, 64, 65, 70, 75–83), which are some of the cancer types where RhoA is also overexpressed. Although the link between HO-1 expression and aberrant cell growth is starting to be unraveled, metalloporphyrins that inhibit HO-1 deserve further studies as antitumoral drugs.

Several recent studies show an important role for HO-1 and the products derived from its enzymatic activity (carbon monoxide, iron, and biliverdin) in the synthesis of VEGF and angiogenesis (3, 59, 70, 77, 78). VEGF is a well known determinant factor in the development of tumorigenesis induced by vGPCR (23, 54), and we have shown that HO-1 mediates vGPCR-induced VEGF-A expression (25). In this study, we show that cells expressing RhoA and tumors derived from them display VEGF-A expression and secretion levels similar to those found in vGPCR-expressing cells and vGPCR-induced tumors. It is noteworthy that the impairment of RhoA expression in vGPCR-expressing cells reduced VEGF-A secretion, and treatment with SnPP strongly reduced VEGF-A expression in RhoA-derived tumors. These data support the evidence that RhoA and HO-1 are important mediators in the pathway that connects the viral receptor to VEGF-A expression

and secretion. RhoA activation is also involved in the regulation of VEGF levels in hypoxia (84, 85) and angiogenesis (86, 87), and part of the antiangiogenic and antimetastatic effects of the new candidate antitumoral drugs statins are attributed to their potential to inactivate RhoA and the consequent down-regulation of VEGF levels (88, 89).

In conclusion, our data show that vGPCR induces HO-1 expression through a pathway that involves $G\alpha_{12}$, $G\alpha_{13}$, and RhoA. Blockage of these $G\alpha$ subunits, RhoA or HO-1 expression, and/or activity results in strongly reduced vGPCR-induced cell transformation and tumor growth. These results help uncovering the complex nature of the signaling pathways regulated by vGPCR and reinforce the notion of HO-1 as a potential therapeutic target in the treatment of KS as well as in other tumors that display elevated RhoA expression and activity.

*Acknowledgments—We thank Dr. Victor Calvo, Carla Mazzeo, and Dr. Manuel Izquierdo for support and help with this work and Drs. Mario Chiariello, Alejandro Curino, and M. Marta Facchinetti for critical reading of the manuscript.*

## REFERENCES


1. Maines, M. D., and Gibbs, P. E. (2005) *Biochem. Biophys. Res. Commun.* **338,** 568–577
2. Alam, J., Igarashi, K., Immenschuh, S., Shibahara, S., and Tyrrell, R. M. (2004) *Antioxid. Redox Signal.* **6,** 924–933
3. Dulak, J., Loboda, A., Zagorska, A., and Jozkowicz, A. (2004) *Antioxid. Redox Signal.* **6,** 858–866
4. Kiemer, A. K., Bildner, N., Weber, N. C., and Vollmar, A. M. (2003) *Endocrinology* **144,** 802–812
5. Lam, C. W., Getting, S. J., and Perretti, M. (2005) *J. Immunol.* **174,** 2297–2304
6. Malaguarnera, L., Imbesi, R. M., Scuto, A., D'Amico, F., Licata, F., Messina, A., and Sanfilippo, S. (2004) *J. Cell. Biochem.* **93,** 197–206
7. Martin, D., Rojo, A. I., Salinas, M., Diaz, R., Gallardo, G., Alam, J., De Galarreta, C. M., and Cuadrado, A. (2004) *J. Biol. Chem.* **279,** 8919–8929
8. Berberat, P. O., Dambrauskas, Z., Gulbinas, A., Giese, T., Giese, N., Kunzli, B., Autschbach, F., Meuer, S., Buchler, M. W., and Friess, H. (2005) *Clin. Cancer Res.* **11,** 3790–3798
9. Fang, J., Akaike, T., and Maeda, H. (2004) *Apoptosis* **9,** 27–35
10. Jazwa, A., Loboda, A., Golda, S., Cisowski, J., Szelag, M., Zagorska, A., Sroczynska, P., Drukala, J., Jozkowicz, A., and Dulak, J. (2006) *Free Radic. Biol. Med.* **40,** 1250–1263
11. Kruger, A. L., Peterson, S. J., Schwartzman, M. L., Fusco, H., McClung, J. A., Weiss, M., Shenouda, S., Goodman, A. I., Goligorsky, M. S., Kappas, A., and Abraham, N. G. (2006) *J. Pharmacol. Exp. Ther.* **319,** 1144–1152
12. Mayerhofer, M., Florian, S., Krauth, M. T., Aichberger, K. J., Bilban, M., Marculescu, R., Printz, D., Fritsch, G., Wagner, O., Selzer, E., Sperr, W. R., Valent, P., and Sillaber, C. (2004) *Cancer Res.* **64,** 3148–3154
13. Sunamura, M., Duda, D. G., Ghattas, M. H., Lozonschi, L., Motoi, F., Yamauchi, J., Matsuno, S., Shibahara, S., and Abraham, N. G. (2003) *Angiogenesis* **6,** 15–24
14. Was, H., Cichon, T., Smolarczyk, R., Rudnicka, D., Stopa, M., Chevalier, C., Leger, J. J., Lackowska, B., Grochot, A., Bojkowska, K., Ratajska, A., Kieda, C., Szala, S., Dulak, J., and Jozkowicz, A. (2006) *Am. J. Pathol.* **169,** 2181–2198
15. McAllister, S. C., Hansen, S. G., Ruhl, R. A., Raggo, C. M., DeFilippis, V. R., Greenspan, D., Fruh, K., and Moses, A. V. (2004) *Blood* **103,** 3465–3473
16. Flore, O., Rafii, S., Ely, S., O'Leary, J. J., Hyjek, E. M., and Cesarman, E. (1998) *Nature* **394,** 588–592
17. Montaner, S., Sodhi, A., Molinolo, A., Bugge, T. H., Sawai, E. T., He, Y., Li, Y., Ray, P. E., and Gutkind, J. S. (2003) *Cancer Cell* **3,** 23–36
18. Montaner, S., Sodhi, A., Ramsdell, A. K., Martin, D., Hu, J., Sawai, E. T., and Gutkind, J. S. (2006) *Cancer Res.* **66,** 168–174
19. Sodhi, A., Montaner, S., and Gutkind, J. S. (2004) *FASEB J.* **18,** 422–427
20. Jensen, K. K., Manfra, D. J., Grisotto, M. G., Martin, A. P., Vassileva, G., Kelley, K., Schwartz, T. W., and Lira, S. A. (2005) *J. Immunol.* **174,** 3686–3694
21. Mutlu, A. D., Cavallin, L. E., Vincent, L., Chiozzini, C., Eroles, P., Duran, E. M., Asgari, Z., Hooper, A. T., La Perle, K. M., Hilsher, C., Gao, S. J., Dittmer, D. P., Rafii, S., and Mesri, E. A. (2007) *Cancer Cell* **11,** 245–258
22. Arvanitakis, L., Geras-Raaka, E., Varma, A., Gershengorn, M. C., and Cesarman, E. (1997) *Nature* **385,** 347–350
23. Bais, C., Santomasso, B., Coso, O., Arvanitakis, L., Raaka, E. G., Gutkind, J. S., Asch, A. S., Cesarman, E., Gershengorn, M. C., and Mesri, E. A. (1998) *Nature* **391,** 86–89
24. Yang, T. Y., Chen, S. C., Leach, M. W., Manfra, D., Homey, B., Wiekowski, M., Sullivan, L., Jenh, C. H., Narula, S. K., Chensue, S. W., and Lira, S. A. (2000) *J. Exp. Med.* **191,** 445–454
25. Marinissen, M. J., Tanos, T., Bolos, M., de Sagarra, M. R., Coso, O. A., and Cuadrado, A. (2006) *J. Biol. Chem.* **281,** 11332–11346
26. Polson, A. G., Wang, D., DeRisi, J., and Ganem, D. (2002) *Cancer Res.* **62,** 4525–4530
27. Cannon, M. L., and Cesarman, E. (2004) *Oncogene* **23,** 514–523
28. Dadke, D., Fryer, B. H., Golemis, E. A., and Field, J. (2003) *Cancer Res.* **63,** 8837–8847
29. Shepard, L. W., Yang, M., Xie, P., Browning, D. D., Voyno-Yasenetskaya, T., Kozasa, T., and Ye, R. D. (2001) *J. Biol. Chem.* **276,** 45979–45987
30. Hall, A. (2005) *Biochem. Soc. Trans.* **33,** 891–895
31. Montaner, S., Sodhi, A., Servitja, J. M., Ramsdell, A. K., Barac, A., Sawai, E. T., and Gutkind, J. S. (2004) *Blood* **104,** 2903–2911
32. Ishizaka, N., and Griendling, K. K. (1997) *Hypertension* **29,** 790–795
33. Matsuoka, Y., Kitamura, Y., Kakimura, J., and Taniguchi, T. (1999) *Neuropharmacology* **38,** 825–834
34. Sun, J., Kim, S. J., Park, M. K., Kim, H. J., Tsoy, I., Kang, Y. J., Lee, Y. S., Seo, H. G., Lee, J. H., and Chang, K. C. (2005) *FEBS Lett.* **579,** 5494–5500
35. Goldhar, A. S., Vonderhaar, B. K., Trott, J. F., and Hovey, R. C. (2005) *Mol. Cell. Endocrinol.* **232,** 9–19
36. Rojo, A. I., Salina, M., Salazar, M., Takahashi, S., Suske, G., Calvo, V., de Sagarra, M. R., and Cuadrado, A. (2006) *Free Radic. Biol. Med.* **41,** 247–261
37. Chikumi, H., Vazquez-Prado, J., Servitja, J. M., Miyazaki, H., and Gutkind, J. S. (2002) *J. Biol. Chem.* **277,** 27130–27134
38. Marinissen, M. J., Chiariello, M., Tanos, T., Bernard, O., Narumiya, S., and Gutkind, J. S. (2004) *Mol. Cell* **14,** 29–41
39. Marinissen, M. J., and Gutkind, J. S. (2001) *Trends Pharmacol. Sci.* **22,** 368–376
40. Marinissen, M. J., Servitja, J. M., Offermanns, S., Simon, M. I., and Gutkind, J. S. (2003) *J. Biol. Chem.* **278,** 46814–46825
41. Pille, J. Y., Denoyelle, C., Varet, J., Bertrand, J. R., Soria, J., Opolon, P., Lu, H., Pritchard, L. L., Vannier, J. P., Malvy, C., Soria, C., and Li, H. (2005) *Mol. Ther.* **11,** 267–274
42. Shin, K. J., Wall, E. A., Zavzavadjian, J. R., Santat, L. A., Liu, J., Hwang, J. I., Rebres, R., Roach, T., Seaman, W., Simon, M. I., and Fraser, I. D. (2006) *Proc. Natl. Acad. Sci. U. S. A.* **103,** 13759–13764
43. Fukuhara, S., Chikumi, H., and Gutkind, J. S. (2000) *FEBS Lett.* **485,** 183–188
44. Couty, J. P., Geras-Raaka, E., Weksler, B. B., and Gershengorn, M. C. (2001) *J. Biol. Chem.* **276,** 33805–33811
45. Marinissen, M. J., Chiariello, M., and Gutkind, J. S. (2001) *Genes Dev.* **15,** 535–553
46. De Vivo, M., Chen, J., Codina, J., and Iyengar, R. (1992) *J. Biol. Chem.* **267,** 18263–18266
47. Fukuhara, S., Murga, C., Zohar, M., Igishi, T., and Gutkind, J. S. (1999) *J. Biol. Chem.* **274,** 5868–5879
48. Fukuhara, S., Marinissen, M. J., Chiariello, M., and Gutkind, J. S. (2000) *J. Biol. Chem.* **275,** 21730–21736
49. Xu, N., Voyno-Yasenetskaya, T., and Gutkind, J. S. (1994) *Biochem. Biophys. Res. Commun.* **201,** 603–609

50. Fukuhara, S., Chikumi, H., and Gutkind, J. S. (2001) *Oncogene* **20,** 1661–1668
51. Vazquez-Prado, J., Basile, J., and Gutkind, J. S. (2004) *Methods Enzymol.* **390,** 259–285
52. Booden, M. A., Siderovski, D. P., and Der, C. J. (2002) *Mol. Cell. Biol.* **22,** 4053–4061
53. Perona, R., Montaner, S., Saniger, L., Sanchez-Perez, I., Bravo, R., and Lacal, J. C. (1997) *Genes Dev.* **11,** 463–475
54. Bais, C., Van Geelen, A., Eroles, P., Mutlu, A., Chiozzini, C., Dias, S., Silverstein, R. L., Rafii, S., and Mesri, E. A. (2003) *Cancer Cell* **3,** 131–143
55. Fromm, C., Coso, O. A., Montaner, S., Xu, N., and Gutkind, J. S. (1997) *Proc. Natl. Acad. Sci. U. S. A.* **94,** 10098–10103
56. Sardana, M. K., and Kappas, A. (1987) *Proc. Natl. Acad. Sci. U. S. A.* **84,** 2464–2468
57. Hamden, K. E., Whitman, A. G., Ford, P. W., Shelton, J. G., McCubrey, J. A., and Akula, S. M. (2005) *Leukemia* **19,** 18–26
58. Sodhi, A., Montaner, S., Patel, V., Zohar, M., Bais, C., Mesri, E. A., and Gutkind, J. S. (2000) *Cancer Res.* **60,** 4873–4880
59. Dulak, J., Jozkowicz, A., Foresti, R., Kasza, A., Frick, M., Huk, I., Green, C. J., Pachinger, O., Weidinger, F., and Motterlini, R. (2002) *Antioxid. Redox Signal.* **4,** 229–240
60. Goodman, A. I., Choudhury, M., da Silva, J. L., Schwartzman, M. L., and Abraham, N. G. (1997) *Proc. Soc. Exp. Biol. Med.* **214,** 54–61
61. Liu, Z. M., Chen, G. G., Ng, E. K., Leung, W. K., Sung, J. J., and Chung, S. C. (2004) *Oncogene* **23,** 503–513
62. Benitah, S. A., Valeron, P. F., van Aelst, L., Marshall, C. J., and Lacal, J. C. (2004) *Biochim. Biophys. Acta* **1705,** 121–132
63. Fritz, G., Just, I., and Kaina, B. (1999) *Int. J. Cancer* **81,** 682–687
64. Gomez del Pulgar, T., Benitah, S. A., Valeron, P. F., Espina, C., and Lacal, J. C. (2005) *BioEssays* **27,** 602–613
65. Pan, Y., Bi, F., Liu, N., Xue, Y., Yao, X., Zheng, Y., and Fan, D. (2004) *Biochem. Biophys. Res. Commun.* **315,** 686–691
66. Sodhi, A., Chaisuparat, R., Hu, J., Ramsdell, A. K., Manning, B. D., Sausville, E. A., Sawai, E. T., Molinolo, A., Gutkind, J. S., and Montaner, S. (2006) *Cancer Cell* **10,** 133–143
67. Sodhi, A., Montaner, S., Patel, V., Gomez-Roman, J. J., Li, Y., Sausville, E. A., Sawai, E. T., and Gutkind, J. S. (2004) *Proc. Natl. Acad. Sci. U. S. A.* **101,** 4821–4826
68. Anderson, K. E., Simionatto, C. S., Drummond, G. S., and Kappas, A. (1984) *J. Pharmacol. Exp. Ther.* **228,** 327–333
69. Brouard, S., Otterbein, L. E., Anrather, J., Tobiasch, E., Bach, F. H., Choi, A. M., and Soares, M. P. (2000) *J. Exp. Med.* **192,** 1015–1026
70. Jozkowicz, A., Huk, I., Nigisch, A., Weigel, G., Weidinger, F., and Dulak, J. (2002) *Antioxid. Redox Signal.* **4,** 577–585
71. Yoshinaga, T., Sassa, S., and Kappas, A. (1982) *J. Biol. Chem.* **257,** 7778–7785
72. Cornelius, C. E., and Rodgers, P. A. (1984) *Pediatr. Res.* **18,** 728–730
73. Devesa, I., Ferrandiz, M. L., Terencio, M. C., Joosten, L. A., van den Berg, W. B., and Alcaraz, M. J. (2005) *Arthritis Rheum.* **52,** 3230–3238
74. Kappas, A., Drummond, G. S., and Valaes, T. (2001) *Pediatrics* **108,** 25–30
75. Drummond, G. S., and Kappas, A. (2004) *Semin. Perinatol.* **28,** 365–368
76. Doi, K., Akaike, T., Fujii, S., Tanaka, S., Ikebe, N., Beppu, T., Shibahara, S., Ogawa, M., and Maeda, H. (1999) *Br. J. Cancer* **80,** 1945–1954
77. Bussolati, B., and Mason, J. C. (2006) *Antioxid. Redox Signal.* **8,** 1153–1163
78. Cisowski, J., Loboda, A., Jozkowicz, A., Chen, S., Agarwal, A., and Dulak, J. (2005) *Biochem. Biophys. Res. Commun.* **326,** 670–676
79. Caballero, F., Meiss, R., Gimenez, A., Batlle, A., and Vazquez, E. (2004) *Int. J. Exp. Pathol.* **85,** 213–222
80. Chen, G. G., Liu, Z. M., Vlantis, A. C., Tse, G. M., Leung, B. C., and van Hasselt, C. A. (2004) *J. Cell. Biochem.* **92,** 1246–1256
81. Nishie, A., Ono, M., Shono, T., Fukushi, J., Otsubo, M., Onoue, H., Ito, Y., Inamura, T., Ikezaki, K., Fukui, M., Iwaki, T., and Kuwano, M. (1999) *Clin. Cancer Res.* **5,** 1107–1113
82. Okamoto, I., Krogler, J., Endler, G., Kaufmann, S., Mustafa, S., Exner, M., Mannhalter, C., Wagner, O., and Pehamberger, H. (2006) *Int. J. Cancer* **119,** 1312–1315
83. Yanagawa, T., Omura, K., Harada, H., Nakaso, K., Iwasa, S., Koyama, Y., Onizawa, K., Yusa, H., and Yoshida, H. (2004) *Oral. Oncol.* **40,** 21–27
84. Turcotte, S., Desrosiers, R. R., and Beliveau, R. (2003) *J. Cell Sci.* **116,** 2247–2260
85. Wojciak-Stothard, B., Tsang, L. Y., Paleolog, E., Hall, S. M., and Haworth, S. G. (2006) *Am. J. Physiol.* **290,** L1173–L1182
86. Hoang, M. V., Whelan, M. C., and Senger, D. R. (2004) *Proc. Natl. Acad. Sci. U. S. A.* **101,** 1874–1879
87. van Nieuw Amerongen, G. P., Koolwijk, P., Versteilen, A., and van Hinsbergh, V. W. (2003) *Arterioscler. Thromb. Vasc. Biol.* **23,** 211–217
88. Xu, H., Zeng, L., Peng, H., Chen, S., Jones, J., Chew, T. L., Sadeghi, M. M., Kanwar, Y. S., and Danesh, F. R. (2006) *Am. J. Physiol.* **291,** F995–F1004
89. Zeng, L., Xu, H., Chew, T. L., Eng, E., Sadeghi, M. M., Adler, S., Kanwar, Y. S., and Danesh, F. R. (2005) *FASEB J.* **19,** 1845–1847